

University of Nebraska - Lincoln

DigitalCommons@University of Nebraska - Lincoln

Papers in the Earth and Atmospheric Sciences

Earth and Atmospheric Sciences, Department
of

6-13-2021

pyUserCalc: A Revised Jupyter Notebook Calculator for Uranium-Series Disequilibria in Basalts

Lynne J. Elkins

Marc Spiegelman

Follow this and additional works at: <https://digitalcommons.unl.edu/geosciencefacpub>



Part of the [Earth Sciences Commons](#)

This Article is brought to you for free and open access by the Earth and Atmospheric Sciences, Department of at DigitalCommons@University of Nebraska - Lincoln. It has been accepted for inclusion in Papers in the Earth and Atmospheric Sciences by an authorized administrator of DigitalCommons@University of Nebraska - Lincoln.

Earth and Space Science



**TECHNICAL
REPORTS: METHODS**
10.1029/2020EA001619

pyUserCalc: A Revised Jupyter Notebook Calculator for Uranium-Series Disequilibria in Basalts

Lynne J. Elkins¹  and Marc Spiegelman² 

¹University of Nebraska-Lincoln, Lincoln, NE, USA, ²Lamont-Doherty Earth Observatory of Columbia University, Palisades, NY, USA

Key Points:

- Cloud-based Jupyter notebook presents an open source, reproducible tool for modeling U-series in basalts
- Equilibrium and pure disequilibrium porous flow U-series models with 1D conservation of mass
- Scaled porous flow model introduces incomplete equilibrium scenario with reaction rate limitations

Supporting Information:

Supporting Information may be found in the online version of this article.

Correspondence to:

L. J. Elkins,
ljelkins@unl.edu

Citation:

Elkins, L. J., & Spiegelman, M. (2021). pyUserCalc: A revised Jupyter notebook calculator for uranium-series disequilibria in basalts. *Earth and Space Science*, 8, e2020EA001619. <https://doi.org/10.1029/2020EA001619>

Received 22 DEC 2020
Accepted 13 JUN 2021

Abstract Meaningful analysis of uranium-series isotopic disequilibria in basaltic lavas relies on the use of complex forward numerical models like dynamic melting (McKenzie, 1985, [https://doi.org/10.1016/0012-821x\(85\)90001-9](https://doi.org/10.1016/0012-821x(85)90001-9)) and equilibrium porous flow (Spiegelman & Elliott, 1993, [https://doi.org/10.1016/0012-821x\(93\)90155-3](https://doi.org/10.1016/0012-821x(93)90155-3)). Historically, such models have either been solved analytically for simplified scenarios, such as constant melting rate or constant solid/melt trace element partitioning throughout the melting process, or have relied on incremental or numerical calculators with limited power to solve problems and/or restricted availability. The most public numerical solution to reactive porous flow, UserCalc (Spiegelman, 2000, <https://doi.org/10.1029/1999gc000030>) was maintained on a private institutional server for nearly two decades, but that approach has been unsustainable in light of modern security concerns. Here, we present a more long-lasting solution to the problems of availability, model sophistication and flexibility, and long-term access in the form of a cloud-hosted, publicly available Jupyter notebook. Similar to UserCalc, the new notebook calculates U-series disequilibria during time-dependent, equilibrium partial melting in a one-dimensional porous flow regime where mass is conserved. In addition, we also provide a new disequilibrium transport model which has the same melt transport model as UserCalc, but approximates rate-limited diffusive exchange of nuclides between solid and melt using linear kinetics. The degree of disequilibrium during transport is controlled by a Damköhler number, allowing the full spectrum of equilibration models from complete fractional melting ($Da = 0$) to equilibrium transport ($Da = \infty$).

Access the full executable Jupyter notebook version of this manuscript here



1. Introduction

Continuous forward melting models are necessary to interpret the origins of empirically measured U-series isotopic disequilibria in basaltic lavas, but the limited and unreliable availability of reproducible tools for making such calculations remains a persistent problem for geochemists. To date, a number of models have been developed for this task, including classical dynamic melting after McKenzie (1985) and the reactive porous flow model of Spiegelman and Elliott (1993). There have since been numerous approaches to using both the dynamic and porous flow models that range from simplified analytical solutions (e.g., Sims et al., 1999; Zou & Zindler, 2000) to incremental dynamic melting calculators (Stracke et al., 2003), two-porosity calculators (Jull et al., 2002; Lundstrom et al., 2000; Sims et al., 2002), and one-dimensional numerical solutions to reactive porous flow (Spiegelman, 2000) and dynamic melting (Bourdon et al., 2005; Elkins et al., 2019). Unfortunately, some of the approaches published since 1990 lacked publicly available tools that would permit others to directly apply the authors' methods, and while the more simplified and incremental approaches remain appropriate for asking and approaching some questions, they are insufficient for other applications that require more complex approaches (e.g., two-lithology melting; Elkins et al., 2019). Other tools like UserCalc that were available to public users (Spiegelman, 2000) were limited in application and have since become unavailable.

In light of the need for more broadly accessible and flexible solutions to U-series disequilibrium problems in partial melting, here we present a cloud-server hosted, publicly available numerical calculator for one-dimensional, decompression partial melting. The tool is provided in a Jupyter notebook with importable Python code and can be accessed from a web browser. Users will be able to access and use the tool using a free cloud server account, or on their own computer given any standard Python distribution. As shown below, the notebook is structured to permit the user to select one of two primary model versions, either classical reactive porous flow after Spiegelman and Elliott (1993) and Spiegelman (2000), or a new disequilibrium transport model, developed after the

© 2021 The Authors.

This is an open access article under the terms of the [Creative Commons Attribution-NonCommercial License](https://creativecommons.org/licenses/by-nc/4.0/), which permits use, distribution and reproduction in any medium, provided the original work is properly cited and is not used for commercial purposes.

appendix formulas of Spiegelman and Elliott (1993). The new model ranges from pure disequilibrium porous flow transport (i.e., the mass-conserved equivalent of true fractional melting over time) to a “scaled” disequilibrium scenario, where the degree of chemical equilibrium that is reached is determined by the relationship between the rate of chemical reaction and the solid decompression rate (which is, in turn, related to the overall melting rate), in the form of a Damköhler number.

This scaled disequilibrium model resembles the classic dynamic melting model of McKenzie (1985), with the caveat that ours is the first U-series melting model developed for near-fractional, disequilibrium transport where mass is also conserved within a one-dimensional melting regime. That is, rather than controlling the quantity of melt that remains in equilibrium with the solid using a fixed residual porosity, the melt porosity is controlled by Darcy’s Law and mass conservation constraints after Spiegelman and Elliott (1993), and the “near-fractional” scenario is simulated using the reaction rate of the migrating liquid with the upwelling solid matrix.

2. Calculating U-Series in Basalts During Mass-Conserved, One-Dimensional Porous Flow

2.1. Solving for Equilibrium Transport

Here, we consider several forward melting models that calculate the concentrations and activities of U-series isotopes (^{238}U , ^{230}Th , ^{226}Ra , ^{235}U , and ^{231}Pa) during partial melting and melt transport due to adiabatic mantle decompression. Following Spiegelman and Elliott (1993), we start with conservation of mass equations for the concentration of a nuclide i , assuming chemical equilibrium between melt and solid:

$$\frac{\partial}{\partial t}[\rho_f\phi + \rho_s(1 - \phi)D_i]c_i^f + \nabla \cdot [\rho_f\phi v + \rho_s(1 - \phi)D_iV]c_i^f = \lambda_{i-1}[\rho_f\phi + \rho_s(1 - \phi)D_{i-1}]c_{i-1}^f - \lambda_i[\rho_f\phi + \rho_s(1 - \phi)D_i]c_i^f \quad (1)$$

where t is time, c_i^f is the concentration of nuclide i in the melt, D_i is the bulk solid/liquid partition coefficient for nuclide i , ρ_f is the density of the fluid and ρ_s is the density of the solid, ϕ is the porosity (local volume fraction of melt), v is the velocity of the melt and V the velocity of the solid in three dimensions, λ_i is the decay constant of nuclide i , and $(i - 1)$ indicates the radioactive parent of nuclide i see Table 1. Equation 1 states that the change in total mass of nuclide i in both the melt and the solid is controlled by the divergence of the mass flux transported by both phases and by the radioactive decay of both parent and daughter nuclides (i.e., the right hand side of the equation above).

The equilibrium model of Spiegelman and Elliott (1993) assumes that complete chemical equilibrium is maintained between the migrating partial melt and the solid rock matrix along a decompressing one-dimensional column. To close the equations, they assume that melt transport is described by a simplified form of Darcy’s Law for permeable flow through the solid matrix. In one dimension, for a steady-state upwelling column of melting mantle rocks, they defined the one-dimensional melt and solid velocities (w and W , respectively), and expressed the melt and solid fluxes as functions of height (z) in terms of a constant melting rate Γ_0 :

$$\rho_f\phi w = \Gamma_0 z \quad (2)$$

$$\rho_s(1 - \phi)W = \rho_s W_0 - \Gamma_0 z \quad (3)$$

where W_0 is the solid mantle upwelling rate, and Γ_0 is equivalent to $\rho_s W_0 F_{max}$ divided by the depth h for a maximum degree of melting F_{max} .

Assuming an initial condition of secular equilibrium, where the initial activities $\lambda_i c_{i,0}^f D_i$ are equivalent for parent and daughter nuclides, they derived a system of differential equations for the concentration c_i^f in any decay chain, which can be solved numerically using Equation 10 from Spiegelman and Elliott (1993):

Table 1
List of Variables Used in This Study

Variable	Definition
c_i^f	Concentration of nuclide i in the liquid
c_i^s	Concentration of nuclide i in the solid
U_i^f	Natural log of the concentration of nuclide i in the liquid relative to its initial concentration
U_i^s	Natural log of the concentration of nuclide i in the solid relative to its initial concentration
U_i^{stable}	Stable element component of U_i^f
U_i^{rad}	Radiogenic component of U_i^f
a_i	Activity of nuclide i
a_i^0	Initial activity of nuclide i
z	Height in a one-dimensional melting column
h	Total height of the melting column
ζ	$= z/h$, Dimensionless fractional height in scaled one-dimensional melting column
D_i	Bulk solid/liquid partition coefficient for nuclide i
D_i^0	Initial bulk solid/liquid partition coefficient for nuclide i
ρ_f	Density of the liquid
ρ_s	Density of the solid
ϕ	Porosity (volume fraction of liquid present)
ϕ_0	Maximum or reference porosity
V	Solid velocity
v	Liquid velocity
W	One-dimensional solid velocity
w	One-dimensional liquid velocity
W_0	Solid mantle upwelling velocity
λ_i	Decay constant for nuclide i
λ_i'	$= \lambda_i h / W_0$, Decay constant for nuclide i scaled by solid transport time
Γ	Melting rate
Γ_0	Constant melting rate
F_{max}	Maximum degree of melting
w_{eff}^i	Effective liquid velocity of nuclide i
R_i^{i-1}	Ingrowth factor
α_i^0	Initial degree of secular disequilibrium in the unmelted solid
k	Permeability
K_r	Relative permeability factor
n	Permeability exponent
A_d	Permeability calibration function
\mathfrak{R}	Reactivity rate factor
d	Diffusion/reaction length scale (e.g., grain-size)
Da	Damköhler number

$$\frac{dc'_i}{d\zeta} = c'_i \frac{(D_i - 1)F_{max}}{D_i + (1 - D_i)F_{max}\zeta} + \lambda_i h \left[\frac{D_i[D_{i-1} + (1 - D_{i-1})F_{max}\zeta]}{D_{i-1}[D_i + (1 - D_i)F_{max}\zeta]} \frac{c'_{i-1}}{w_{eff}^{i-1}} - \frac{c'_i}{w_{eff}^i} \right] \quad (4)$$

where c'_i is the scaled melt concentration ($= c_i^f/c_{i,0}^f$), ζ is the dimensionless fractional height in the scaled column, equal to 0 at the base and 1 at the top, and

$$w_{eff}^i = \frac{\rho_f \phi w + \rho_s (1 - \phi) D_i W}{\rho_f \phi + \rho_s (1 - \phi) D_i} \quad (5)$$

is the effective velocity for element i .

In their appendix, Spiegelman and Elliott (1993) developed the more general (and, arguably, realistic) form where Γ and D_i are functions of height z . The UserCalc model of Spiegelman (2000) then formulated a one-dimensional numerical integration for the concentrations of selected U-series isotopes in continuously produced partial melts with height z , after the equilibrium formulas above. The concentration expression derived by Spiegelman (2000) for the equilibrium scenario (Formula 6 in that reference) is:

$$\frac{dc_i^f}{dz} = \frac{-c_i^f(z)}{F(z) + (1 - F(z))D_i(z)} \frac{d}{dz} [F(z) + (1 - F(z))D_i(z)] + \frac{\lambda_{i-1} \overline{\rho D_{i-1}} c_{i-1}^f(z) - \lambda_i \overline{\rho D_i} c_i^f(z)}{\rho_s W_0 [F(z) + (1 - F(z))D_i(z)]} \quad (6)$$

where F is the degree of melting. Spiegelman (2000) further observed that solving for the natural log of the concentrations normalized to the initial concentration of i , U_i , rather than the concentrations themselves, is more accurate, particularly for highly incompatible elements (Formulas 7–9 of Spiegelman [2000]). This is because log concentrations change linearly during melting, rather than exponentially, and are more numerically stable to calculate.

$$U_i^f = \ln \left(\frac{c_i^f}{c_{i,0}^f} \right) \quad (7)$$

$$\frac{dU_i^f}{dz} = \frac{1}{c_i^f(z)} \frac{dc_i^f}{dz} \quad (8)$$

$$\frac{dU_i^f}{dz} = \frac{-1}{F(z) + (1 - F(z))D_i(z)} \frac{d}{dz} [F(z) + (1 - F(z))D_i(z)] + \frac{\lambda_i}{w_{eff}^i} [R_i^{i-1} \exp[U_{i-1}^f(z) - U_i^f(z)] - 1] \quad (9)$$

For the formulas above, Spiegelman (2000) defined a series of variables that allow for simpler integration formulas and aid in efficient solution of the model, namely

$$\overline{\rho D_i} = \rho_f \phi + \rho_s (1 - \phi) D_i(z), \quad (10)$$

$$\overline{F} = F(z) + (1 - F(z))D_i(z), \quad (11)$$

$$R_i^{i-1} = \alpha_i^0 \frac{D_i^0}{D_{i-1}^0} \frac{\overline{\rho D_{i-1}}}{\overline{\rho D_i}}, \quad (12)$$

$$\alpha_i^0 = \frac{\lambda_{i-1} c_{(i-1),0}^s}{\lambda_i c_{i,0}^s}, \quad (13)$$

and substituting from the formulas above

$$w_{eff}^i = \frac{\rho_s W_0 \overline{F}}{\overline{\rho D_i}}. \quad (14)$$

where D_i^0 is the initial bulk solid/melt partition coefficient for element i , R_i^{i-1} is the ingrowth factor, and α_i^0 is the initial degree of secular disequilibrium for element i in the unmelted solid.

$U_i(z) = \ln(c_f(z)/c_f^0)$, the log of the total concentration of nuclide i in the melt, can then be decomposed into

$$U_i(z) = U_i^{stable}(z) + U_i^{rad}(z) \quad (15)$$

where

$$U_i^{stable}(z) = \ln \left[\frac{D_i^0}{\overline{FD}_i(z)} \right] \quad (16)$$

is the log concentration of a stable nuclide with the same partition coefficients, and $U_i^{rad}(z)$ is the radiogenic ingrowth component. An alternate way of writing the radiogenic ingrowth component of Equation 9 of Spiegelman (2000) is:

$$\frac{dU_i^{rad}}{d\zeta} = \lambda_i' \frac{\overline{\rho D}_i}{\overline{FD}_i} \left[R_i^{i-1} \exp[U_{i-1}(\zeta) - U_i(\zeta)] - 1 \right] \quad (17)$$

where

$$\lambda_i' = \frac{h\lambda_i}{W_0} \quad (18)$$

is the decay constant of nuclide i , scaled by the solid transport time (h/W_0) across a layer of total height h . Note Equation 17 is solved over a column of dimensionless height 1 where $\zeta \in [0,1]$.

Using these equations, the UserCalc reactive porous flow calculator accepted user inputs for both $F(z)$ and $D_i(z)$. The method uses a formula for the melt porosity ($\phi(z)$) based on a Darcy's Law expression with a scaled permeability factor (Formula 20 from Spiegelman [2000]):

$$K_r(z)A_d\phi^n(1-\phi)^2 + \phi \left[1 + F(z) \left(\frac{\rho_s}{\rho_f} - 1 \right) \right] - \frac{\rho_s}{\rho_f} F(z) = 0 \quad (19)$$

where $K_r(z)$ is the scaled permeability with height z , A_d is a permeability calibration function, and n is the permeability exponent. The permeability exponent for a tube-shaped fluid network is expected to be $n = 2$, while for a sheet-shaped network it is $n = 3$; recent measurements of the permeabilities of experimental magmatic melt networks suggest realistic magma migration occurs in a manner intermediate between these two scenarios, with $n = 2.6$ (Miller et al., 2014). The relative permeability K_r is calculated with respect to the permeability at the top of the column, that is, depth $z = z_{final}$:

$$K_r(z) = \frac{k(z)}{k(z_{final})} \quad (20)$$

and allows for locally enhanced flow (e.g., mimicking the effects of a relatively low viscosity fluid).

Our model implementation reproduces and builds on the prior efforts summarized above, using a readily accessible computer language (Python) and web application (Jupyter notebooks).

2.2. Solving for Complete Disequilibrium Transport

We further present a calculation tool that solves a similar set of equations for pure chemical disequilibrium transport during one-dimensional decompression melting. This model assumes that the solid produces an instantaneous fractional melt in local equilibrium with the solid; however, the melt is not allowed to back-react with the solid during transport, as it would in the equilibrium model above. In the limiting condition defined by stable trace elements (i.e., without radioactive decay), the model reduces to the calculation for an accumulated fractional

melt. The model solves for the concentration of each nuclide i in the solid (s) and liquid (f) using Equations 26 and 27 of Spiegelman and Elliott (1993):

$$\frac{dc_i^s}{dz} = \frac{c_i^s(z) \left(1 - \frac{1}{D_i(z)}\right)}{1 - F(z)} \frac{dF}{dz} + \frac{1 - \phi}{W_0(1 - F(z))} [\lambda_{i-1} c_{i-1}^s(z) - \lambda_i c_i^s(z)] \quad (21)$$

$$\frac{dc_i^f}{dz} = \frac{\frac{c_i^s(z)}{D_i(z)} - c_i^f(z)}{F(z)} \frac{dF}{dz} + \frac{\rho_f \phi}{\rho_s W_0 F(z)} [\lambda_{i-1} c_{i-1}^f(z) - \lambda_i c_i^f(z)] \quad (22)$$

which maintain conservation of mass for both fluid and solid individually, and do not assume chemical equilibration between the two phases. As above, the equations depend on $F(z)$ and $D_i(z)$, that is, melt fractions and bulk rock partition coefficients that can vary with depth.

As above, the solid and fluid concentration equations are rewritten in terms of the logs of the concentrations:

$$U_i^s(z) = \ln \left(\frac{c_i^s(z)}{c_{i,0}^s} \right), \quad U_i^f(z) = \ln \left(\frac{c_i^f(z)}{c_{i,0}^f} \right) \quad (23)$$

and thus

$$\frac{dU_i}{dz} = \frac{1}{c_i(z)} \frac{dc_i}{dz} \quad (24)$$

We assume that initial $c_{i,0}^s = D_{i,0} c_{i,0}^f$. Also as above, the log concentration equations can be broken into stable and radiogenic components, where the stable log concentration equations are:

$$\frac{dU_i^{s,stable}}{dz} = \frac{1 - \frac{1}{D_i(z)}}{1 - F(z)} \frac{dF}{dz} \quad (25)$$

$$\frac{dU_i^{f,stable}}{dz} = \frac{\frac{D_i^0}{D_i(z)} \exp(U_i^s(z) - U_i^f(z))}{F(z)} \frac{dF}{dz} \quad (26)$$

which are equivalent to a model for a fractionally melted residual solid and an accumulated fractional melt for the liquid.

Reincorporating this with the radiogenic component and scaling all distances by h gives the dimensionless equations:

$$\frac{dU_i^s}{d\zeta} = \frac{1 - \frac{1}{D_i(\zeta)}}{1 - F(\zeta)} \frac{dF}{d\zeta} + \frac{1 - \phi}{1 - F(\zeta)} \lambda_i' \left[\frac{\alpha_{i-1}^0}{\alpha_i^0} \exp[U_{i-1}^s(\zeta) - U_i^s(\zeta)] - 1 \right] \quad (27)$$

$$\frac{dU_i^f}{d\zeta} = \frac{\frac{D_i^0}{D_i(\zeta)} \exp(U_i^s(\zeta) - U_i^f(\zeta))}{F(\zeta)} + \frac{\rho_f \phi}{\rho_s F(\zeta)} \lambda_i' \left[\frac{D_i^0 \alpha_{i-1}^0}{D_{i-1}^0 \alpha_i^0} \exp[U_{i-1}^f(\zeta) - U_i^f(\zeta)] - 1 \right] \quad (28)$$

2.3. Solving for Transport With Chemical Reactivity Rates

The two models described above are end members for complete equilibrium and complete disequilibrium transport. For stable trace elements, these models produce melt compositions that are equivalent to batch melting and

accumulated fractional melting (e.g., Spiegelman & Elliott, 1993). However, the actual transport of a reactive fluid (like a melt) through a solid matrix can fall anywhere between these end members depending on the rate of transport and re-equilibration between melt and solid, which can be sensitive to the mesoscopic geometry of melt and solid (e.g., Spiegelman & Kenyon, 1992). In an intermediate scenario, we envision that some reaction occurs, but chemical equilibration is incomplete due to slow reaction rates relative to the differential transport rates for the fluid and solid. If reaction times are sufficiently rapid to achieve chemical exchange over the lengthscale of interest before the liquid segregates, chemical equilibrium can be achieved; but for reactions that occur more slowly than effective transport rates, only partial chemical equilibrium can occur (e.g., Grose & Afonso, 2019; Iwamori, 1993, 1994; Kogiso et al., 2004; Liang & Liu, 2016; Peate & Hawkesworth, 2005; Qin et al., 1992; Yang et al., 2000). Such reaction rates can include, for example, the rate of chemical migration over the distance between high porosity veins or channels (e.g., Aharonov et al., 1995; Jull et al., 2002; Spiegelman, 2000; Stracke & Bourdon, 2009); or, at the grain scale, the solid chemical diffusivity of elements over the diameter of individual mineral grains (e.g., Feineman & DePaolo, 2003; Grose & Afonso, 2019; Oliveira et al., 2020; Qin et al., 1992; Van Orman et al., 2002, 2006).

To model this scaled reactivity scenario, we start with our equations for disequilibrium transport in a steady-state, one-dimensional conservative system, and add a chemical back-reaction term that permits exchange of elements between the fluid and the solid. The reaction term is scaled by a reactivity rate factor, \mathfrak{R} and expressed in $\text{kg/m}^3/\text{yr}$ (i.e., the same units as the melting rate). The reactivity rate thus behaves much like the melting rate by governing the rate of exchange between the solid and liquid phases, effectively scaling the degree to which chemical exchange can occur. This new term could simulate a number of plausible scenarios that would physically limit the rate of chemical exchange by transport along a given distance in a linear manner, such as the movement or diffusion of nuclides through the porous solid matrix between melt channels a given distance apart.

First, returning to the conservation of mass equations for a steady-state, one-dimensional, reactive system of stable trace elements, and using $\Gamma(z)$ to represent the melting rate:

$$\frac{d}{dz} \rho_f \phi w = \Gamma(z) \quad (29)$$

$$\frac{d}{dz} \rho_s (1 - \phi) W = -\Gamma(z) \quad (30)$$

$$\frac{d}{dz} \rho_f \phi w c_i^f(z) = \frac{c_i^s(z)}{D_i(z)} \Gamma(z) - \mathfrak{R} \left(c_i^f(z) - \frac{c_i^s(z)}{D_i(z)} \right) \quad (31)$$

$$\frac{d}{dz} \rho_s (1 - \phi) W c_i^s(z) = -\frac{c_i^s(z)}{D_i(z)} \Gamma(z) + \mathfrak{R} \left(c_i^f(z) - \frac{c_i^s(z)}{D_i(z)} \right) \quad (32)$$

where, for an adiabatic upwelling column,

$$\Gamma(z) = \rho_s W_0 \frac{dF}{dz} \quad (33)$$

From this, Equations 29 and 30 can be integrated (with appropriate boundary conditions at $z = 0$) to give

$$\rho_f \phi w = \rho_s W_0 F(z) \quad (34)$$

$$\rho_s (1 - \phi) W = \rho_s W_0 (1 - F(z)) \quad (35)$$

Next, we expand the concentration equations to include the reactivity factor, and substitute the conservation of total mass determined above:

$$\rho_s W_0 F(z) \frac{d}{dz} c_i^f(z) + c_i^f(z) \Gamma(z) = \frac{c_i^s(z)}{D_i(z)} \Gamma(z) - \mathfrak{R} \left(c_i^f(z) - \frac{c_i^s(z)}{D_i(z)} \right) \quad (36)$$

$$\rho_s W_0 (1 - F(z)) \frac{d}{dz} c_i^s(z) - c_i^s(z) \Gamma(z) = -\frac{c_i^s(z)}{D_i(z)} \Gamma(z) + \mathfrak{R} \left(c_i^f(z) - \frac{c_i^s(z)}{D_i(z)} \right) \quad (37)$$

If we then combine the $\Gamma(z)$ terms and rearrange:

$$\rho_s W_0 F(z) \frac{d}{dz} c_i^f(z) = \Gamma(z) \left(\frac{c_i^s(z)}{D_i(z)} - c_i^f(z) \right) - \mathfrak{R} \left(c_i^f(z) - \frac{c_i^s(z)}{D_i(z)} \right) \quad (38)$$

$$\rho_s W_0 (1 - F(z)) \frac{d}{dz} c_i^s(z) = \Gamma(z) c_i^s(z) \left(1 - \frac{1}{D_i(z)} \right) + \mathfrak{R} \left(c_i^f(z) - \frac{c_i^s(z)}{D_i(z)} \right) \quad (39)$$

We can now divide the fluid and solid equations by c_i^f and c_i^s , respectively, and rearrange the W_0 terms:

$$\frac{1}{c_i^f(z)} \frac{dc_i^f}{dz} = \frac{1}{\rho_s W_0 F(z)} \left[\Gamma(z) \left(\frac{c_i^s(z)}{D_i(z) c_i^f(z)} - 1 \right) - \mathfrak{R} \left(1 - \frac{c_i^s(z)}{D_i(z) c_i^f(z)} \right) \right] \quad (40)$$

$$\frac{1}{c_i^s(z)} \frac{dc_i^s}{dz} = \frac{1}{\rho_s W_0 (1 - F(z))} \left[\Gamma(z) \left(1 - \frac{1}{D_i(z)} \right) + \frac{\mathfrak{R}}{D_i(z)} \left(\frac{D_i(z) c_i^f(z)}{c_i^s(z)} - 1 \right) \right] \quad (41)$$

The first terms on the right-hand side of each of these equations are identical to pure disequilibrium melting, such that if \mathfrak{R} is zero, the equations reduce to the disequilibrium transport case of Spiegelman and Elliott (1993).

To solve, the final terms that involve the reactivity factor can be further rewritten using the definitions for U_i^f and U_i^s :

$$c_i^f(z) = c_{i,0}^f \exp[U_i^f(z)] = \frac{c_{i,0}^s}{D_i^0} \exp[U_i^f(z)] \quad (42)$$

$$c_i^s(z) = c_{i,0}^s \exp[U_i^s(z)] \quad (43)$$

Thus:

$$\frac{D_i(z) c_i^f(z)}{c_i^s(z)} = \frac{D_i(z)}{D_i^0} \exp[U_i^f(z) - U_i^s(z)] \quad (44)$$

$$\frac{c_i^s(z)}{D_i(z) c_i^f(z)} = \frac{D_i^0}{D_i(z)} \exp[U_i^s(z) - U_i^f(z)] \quad (45)$$

and:

$$\frac{dU_i^f}{dz} = \frac{1}{\rho_s W_0 F(z)} \left[\Gamma(z) \left(\frac{D_i^0}{D_i(z)} \exp[U_i^s(z) - U_i^f(z)] - 1 \right) - \mathfrak{R} \left(1 - \frac{D_i^0}{D_i(z)} \exp[U_i^s(z) - U_i^f(z)] \right) \right] \quad (46)$$

$$\frac{dU_i^s}{dz} = \frac{1}{\rho_s W_0 (1 - F(z))} \left[\Gamma(z) \left(1 - \frac{1}{D_i(z)} \right) + \frac{\mathfrak{R}}{D_i(z)} \left(\frac{D_i(z)}{D_i^0} \exp[U_i^f(z) - U_i^s(z)] - 1 \right) \right] \quad (47)$$

Finally, substituting adiabatic upwelling and scaling with depth by h , and adding radioactive terms gives the full solutions for the dimensionless equations $dU_i/d\zeta$:

$$\frac{dU_i^f}{d\zeta} = \frac{1}{F(\zeta)} \left[\frac{dF}{d\zeta} \left(\frac{D_i^0}{D_i(\zeta)} \exp[U_i^s(\zeta) - U_i^f(\zeta)] - 1 \right) \right] - \frac{\mathfrak{R}h}{\rho_s W_0 F(\zeta)} \left[1 - \frac{D_i^0}{D_i(\zeta)} \exp[U_i^s(\zeta) - U_i^f(\zeta)] \right] + \frac{\rho_f \phi}{\rho_s F} \lambda'_i \left[\frac{D_i^0 \alpha_{i-1}^0}{D_{i-1}^0 \alpha_i^0} \exp[U_{i-1}^f(\zeta) - U_i^f(\zeta)] - 1 \right] \quad (48)$$

$$\frac{dU_i^s}{d\zeta} = \frac{1}{(1-F(\zeta))} \left[\frac{dF}{d\zeta} \left(1 - \frac{1}{D_i(\zeta)} \right) \right] + \frac{\mathfrak{R}h}{\rho_s W_0 D_i(\zeta) (1-F(\zeta))} \left[\frac{D_i(\zeta)}{D_i^0} \exp[U_i^f(\zeta) - U_i^s(\zeta)] - 1 \right] + \frac{1-\phi}{1-F(\zeta)} \lambda'_i \left[\frac{\alpha_{i-1}^0}{\alpha_i^0} \exp[U_{i-1}^s(\zeta) - U_i^s(\zeta)] - 1 \right] \quad (49)$$

where h is the total height of the melting column.

2.3.1. The Damköhler Number

The dimensionless combination

$$Da = \frac{\mathfrak{R}h}{\rho_s W_0} \quad (50)$$

is the Damköhler number, which governs the reaction rate relative to the solid transport time. Damköhler numbers more generally are used to relate the timescales of chemical reactions to the rates of physical transport in a system. If re-equilibration is limited by solid state diffusion, \mathfrak{R} can be estimated using:

$$\mathfrak{R} \approx \frac{\rho_s \mathcal{D}_i}{d^2} \quad (51)$$

where \mathcal{D}_i is the *solid state* diffusivity of element i , and d is a nominal spacing between melt-channels (this spacing could, for example, be the average grain diameter for grain-scale channels, or 10 cm for closely spaced veins).

In this case (which we will assume for this article), the Damköhler number can be written

$$Da = \frac{\mathcal{D}_i h}{W_0 d^2} \quad (52)$$

Substituting the definition of Da above yields the final dimensionless ordinary differential equations (ODEs) for the disequilibrium transport model:

$$\frac{dU_i^f}{d\zeta} = \frac{1}{F(\zeta)} \left(\frac{dF}{d\zeta} + Da \right) \left(\frac{D_i^0}{D_i(\zeta)} \exp[U_i^s(\zeta) - U_i^f(\zeta)] - 1 \right) + \frac{\rho_f \phi}{\rho_s F(\zeta)} \lambda'_i \left[\frac{D_i^0 \alpha_{i-1}^0}{D_{i-1}^0 \alpha_i^0} \exp[U_{i-1}^f(\zeta) - U_i^f(\zeta)] - 1 \right] \quad (53)$$

$$\frac{dU_i^s}{d\zeta} = \frac{1}{(1-F(\zeta))} \left[\frac{dF}{d\zeta} \left(1 - \frac{1}{D_i(\zeta)} \right) + \frac{Da}{D_i(\zeta)} \left(\frac{D_i(\zeta)}{D_i^0} \exp[U_i^f(\zeta) - U_i^s(\zeta)] - 1 \right) \right] + \frac{1-\phi}{1-F(\zeta)} \lambda'_i \left[\frac{\alpha_{i-1}^0}{\alpha_i^0} \exp[U_{i-1}^s(\zeta) - U_i^s(\zeta)] - 1 \right] \quad (54)$$

with initial conditions $U_i^s = U_i^f = 0$.

In the limit where the Damköhler number approaches zero, the above formulas reduce to pure disequilibrium transport, whereas if Da approaches infinity (i.e., infinitely fast reactivity compared to physical transport), the system approaches equilibrium conditions ($c_i^s \rightarrow D_i c_i^f$).

2.3.2. Initial Conditions

Inspection of Equation 53 shows that for the initial conditions described above and $F(0) = 0$, $\frac{dU_i^f}{d\zeta}$ is ill-defined (at least numerically in a floating-point system). However, taking the limit $\zeta \rightarrow 0$ and applying L'Hôpital's rule yields

$$\lim_{\zeta \rightarrow 0} \frac{dU_i^f}{d\zeta} = \frac{U_i^s(0) - U_i^f(0)}{F'(0)} \left(\frac{dF}{d\zeta} + Da \right) + \lambda_i' \left[\frac{D_i^0 \alpha_{i-1}^0}{D_{i-1}^0 \alpha_i^0} - 1 \right] \quad (55)$$

where

$$U_i^s(0) = \left. \frac{dU_i^s}{d\zeta} \right|_{\zeta=0} \quad (56)$$

$$U_i^f(0) = \left. \frac{dU_i^f}{d\zeta} \right|_{\zeta=0} \quad (57)$$

$$F'(0) = \left. \frac{dF}{d\zeta} \right|_{\zeta=0} \quad (58)$$

The initial radiogenic term also uses the limit from Equation 34:

$$\lim_{\zeta \rightarrow 0} \frac{\rho_f \phi}{\rho_s F} = \frac{W_0}{w(0)} = 1 \quad (59)$$

Rearranging Equation 55 gives the value for $U_i^f(0)$ for $F = 0$ as

$$\lim_{\zeta \rightarrow 0} \frac{dU_i^f}{d\zeta} = \frac{1}{2 + \frac{Da}{F'(0)}} \left[U_i^s(0) \left(1 + \frac{Da}{F'(0)} \right) + \lambda_i' \left[\frac{D_i^0 \alpha_{i-1}^0}{D_{i-1}^0 \alpha_i^0} - 1 \right] \right] \quad (60)$$

3. A pyUserCalc Jupyter Notebook

3.1. Code Design

The `UserCalc` Python package implements both equilibrium and disequilibrium transport models and provides a set of code classes and utility functions for calculating and visualizing the results of one-dimensional, steady-state, partial melting forward models for both the ^{238}U and ^{235}U decay chains. The code package is organized into a set of Python classes and plotting routines, which are documented in the docstrings of the classes and also demonstrated in detail below. Here we briefly describe the overall functionality and design of the code, which is open-source and can be modified to suit an individual researcher's needs. The code is currently available in a Git repository (<https://gitlab.com/ENKI-portal/pyUsercalc>), and any future edits or merge requests will be managed through GitLab.

The equilibrium and disequilibrium transport models described above have each been implemented as Python classes with a generic code interface:

```

...
Interface:
-----
    model (alpha0, lambdas, D, W0, F, dFdZ, phi, rho_f=2800., rho_s=3300.,
          method=method, Da=inf)

Parameters:
-----
    alpha0 : numpy array of initial activities
    lambdas : numpy array of decay constants scaled by solid transport
              time
    D       : Function D(z) -- returns an array of partition coefficients
              at scaled height z
    W0      : float -- Solid mantle upwelling rate
    F       : Function F(z) -- returns the degree of melting
    dFdZ    : Function dFdZ(z) -- returns the derivative of F
    phi     : Function phi(z) -- returns the porosity
    rho_f   : float -- melt density
    rho_s   : float -- solid density
    method  : string -- ODE time-stepping scheme to be passed to solve_ivp
              (one of 'RK45', 'Radau', 'BDF')
    Da      : float -- Damkohler Number (defaults to \inf, unused in equi-
              librium model)

Required Method:
-----
    model.solve(): returns depth and log concentration numpy arrays z,
                   Us, Uf
...

```

which solves the scaled equations (i.e., Equation 9 or Equations 53 and 54 for the log concentrations of nuclides U_i^f and U_i^s in a decay chain of arbitrary length, with scaled decay constants λ_i and initial activity ratios α_i^0). In the code, we use the variable z for the scaled height in the column (i.e., $z \equiv \zeta$), and the model equations assume a one-dimensional column with scaled height $0 \leq z \leq 1$. The bulk partition coefficients $D_i(z)$, degree of melting $F(z)$, melting rate $dF/dz(z)$, and porosity $\phi(z)$ are provided as functions of height in the column. Optional arguments include the melt and solid densities ρ_f and ρ_s , the Damköhler number Da , and the preferred numerical integration method (see `scipy.integrate.solve_ivp`). Some of these variables, such as $D_i(z)$ and $F(z)$, are provided by the user as described further below, and are then interpolated using model functions.

`UserCalc` provides two separate model classes, `EquilTransport` and `DisequilTransport`, for the different transport models; the user could add any other model that uses the same interface, if desired. Most users, however, will not access the models directly but rather through the driver class `UserCalc`. `UserCalc`, which provides support for solving and visualizing column models for the relevant ^{238}U and ^{235}U decay chains. The general interface for the `UserCalc` class is:

```

...
A class for constructing solutions for 1-D, steady-state, open-system
  U-series transport calculations as in Spiegelman (2000) and
  this study.

Usage:
-----
    us = UserCalc(df,dPdZ = 0.32373,n = 2.,tol=1.e-6,phi0 = 0.008,
                  W0 = 3.,model=EquilTransport, Da=None, stable=False,
                  method='Radau')

Parameters:
-----
df      : A pandas dataframe with columns ['P','F',
      Kr','DU','DTh','DRa','DPa']
dPdZ   : float -- Pressure gradient, to convert pressure P to depth z
n       : float -- Permeability exponent
tol     : float -- Tolerance for the ODE solver
phi0    : float -- Reference melt porosity
W0      : float -- Upwelling velocity (cm/yr)
model   : class -- A U-series transport model class (one of EquilTrans-
      port or DisequilTransport)
Da      : float -- Optional Da number for disequilibrium transport model
stable  : bool
True    : calculates concentrations for non-radiogenic nuclides with
      same chemical properties (i.e., sets lambda=0)
False   : calculates the full radiogenic problem
method  : string
      ODE time-stepping method to pass to solve_ivp (usually one of 'Radau',
      'BDF', or 'RK45')
...

```

The principal required input is a spreadsheet containing the degree of melting $F(P)$, relative permeability $K_r(P)$, and bulk partition coefficients for the elements D_U , D_{Th} , D_{Ra} , and D_{Pa} as functions of pressure P . The structure of the input data spreadsheet is the same as that described in Spiegelman (2000), and is illustrated in Table 2 below. Because the user provides $F(z)$, $K_r(z)$, and bulk solid $D_i(z)$ input information to the model directly, any considerations such as mineral modes, mineral/melt D_i values, and productivity variations are external to this model and must be developed by the user separately. Once given this spreadsheet by the user, the code routine initializes the decay constants for the isotopic decay chains and provides functions to interpolate $F(z)$ and $D_i(z)$ and calculate the porosity $\phi(z)$. Once thus initialized, the `UserCalc` class further provides the following methods:

```

...
Principal Methods:
-----
phi      : returns porosity as a function of column
      height
set_column_parameters : resets principal column parameters phi0, n,
      W0
solve_1D  : 1D column solution for a single Decay chain
      with arbitrary D, lambda, alpha_0
solve_all_1D : Solves a single column model for both 238U
      and 235U chains. returns a pandas dataframe
solve_grid : Solves multiple column models for a grid of
      porosities and upwelling rates returns a 3-D
      array of activity ratios
...

```

Of these, the principal user-facing methods are:

1. `UserCalc.solve_all_1D`, which returns a `pandas.DataFrame` table that contains, at each depth, solutions for the porosity (ϕ), the log concentrations of the specified nuclides in the ^{238}U and ^{235}U decay chains in both the melt and the solid, and the U-series activity ratios.
2. `UserCalc.solve_grid`, which solves for a grid of one-dimensional solutions for different reference porosities (ϕ_0) and solid upwelling rates (W_0) and returns arrays of U-series activity ratios at a specified depth (usually the top of the column), as described in Spiegelman and Elliott (1993).

3.1.1. Visualization Functions

In addition to the principal classes for calculating U-series activity ratios in partial melts, the `UserCalc` package also provides functions for visualizing model inputs and outputs. The primary plotting functions include:

1. `UserCalc.plot_inputs(df)`: Visualizes the input dataframe to show $F(P)$, $K_r(P)$ and $D_i(P)$
2. `UserCalc.plot_1Dcolumn(df)`: Visualizes the output dataframe for a single one-dimensional melting column.
3. `UserCalc.plot_contours(phi0, W0, act)`: Visualizes the output of `UserCalc.solve_grid` by generating contour plots of activity ratios at a specific depth as functions of the porosity (ϕ_0) and solid upwelling rate (W_0).
4. `UserCalc.plot_mesh_Ra(Th, Ra, W0, phi0)` and `UserCalc.plot_mesh_Pa(Th, Pa, W0, phi0)`: Generates “mesh” plots showing results for different ϕ_0 and W_0 values on ($^{226}\text{Ra}/^{230}\text{Th}$) versus ($^{230}\text{Th}/^{238}\text{U}$) and ($^{231}\text{Pa}/^{235}\text{U}$) versus ($^{230}\text{Th}/^{238}\text{U}$) activity diagrams.

Both the primary solver routines and visualization routines will be demonstrated in detail below.

3.1.2. Miscellaneous Convenience Functions

Finally, the `UserCalc` module also provides a simple input spreadsheet generator similar to the one provided with the original `UserCalc` program of Spiegelman (2000). This tool is described more fully in the accompanying Jupyter notebook `twolayermodel.ipynb` in Supporting Information S1, and has the interface:

```
df = UserCalc.twolayermodel(P, F, Kr, D_lower, D_upper, N=100, P_lambda=1)
```

3.2. An Example Demonstrating pyUserCalc Functionality for a Single Melting Column

The Python code cells embedded below provide an example problem that demonstrates the use and behavior of the model for a simple, two-layer upwelling mantle column, with a constant melting rate within each layer and constant $K_r = 1$. This example is used to compare the outcomes from the original `UserCalc` equilibrium model (Spiegelman, 2000) to various other implementations of the code, such as pure disequilibrium transport and scaled reactivity rates, as described above.

To run the example code and use this article as a functioning Jupyter notebook, while in a web-enabled browser the user should select an embedded code cell and then simultaneously type the “Shift” and “Enter” keys to run the cell, after which selection will automatically advance to the following cell. The first cell below imports necessary code libraries to access the Python toolboxes and functions that will be used in the rest of the program:

```
[1]: # Select this cell with by mouseclick, and run the code by simultaneously
      # typing the 'Shift' + 'Enter' keys.
      # If the browser is able to run the Jupyter notebook, a number [1] will
      # appear to the left of the cell.

import pandas as pd
import numpy as np
import matplotlib.pyplot as plt
%matplotlib inline

# Import UserCalc:
import UserCalc
```

3.2.1. Entering Initial Input Information and Viewing Input Data

In the full Jupyter notebook code available in the Git repository and provided here as Supporting Information S1, the user can edit a notebook copy and indicate their initial input data, as has been done for the sample Data Set below. The name for the user's input data file should be set in quotes (i.e., replacing the word "sample" in the cell below with the appropriate filename, minus the file extension). This name will be used both to find the input file and to label any output files produced. Our sample file can likewise be downloaded and used as a formatting template for other input files (see Supporting Information S1), and is presented as a useful example below. The desired input file should be saved to a 'data' folder in the notebook directory prior to running the code. If desired, a similarly simple two-layer input file can also be generated using the calculator tool provided in the supplementary code.

Once the cell has been edited to contain the correct input file name, the user should run the cell using the technique described above:

```
[2]: runname='sample'
```

The next cell below will read in the input data using the user filename specified above:

```
[3]: input_file = 'data/{}.csv'.format(runname)
df = pd.read_csv(input_file, skiprows=1, dtype=float)
df
```

The next cell will visualize the input dataframe in Figure 1, using the utility function `plot_inputs`:

```
[4]: fig = UserCalc.plot_inputs(df)
```

Table 2

Input Data Table for Example Tested Here, Showing Pressures in kbar (P), Degree of Melting (F), Permeability Coefficient (K_p), and Bulk Solid/Melt Partition Coefficients (D_i) for the Elements of Interest, U, Th, Ra, and Pa

	P	F	Kr	DU	DTh	DRa	DPa
0	40.0	0.00000	1.0	0.00900	0.00500	0.00002	0.00001
1	39.0	0.00241	1.0	0.00900	0.00500	0.00002	0.00001
2	38.0	0.00482	1.0	0.00900	0.00500	0.00002	0.00001
3	37.0	0.00723	1.0	0.00900	0.00500	0.00002	0.00001
4	36.0	0.00964	1.0	0.00900	0.00500	0.00002	0.00001
5	35.0	0.01210	1.0	0.00900	0.00500	0.00002	0.00001
6	34.0	0.01450	1.0	0.00900	0.00500	0.00002	0.00001
7	33.0	0.01690	1.0	0.00900	0.00500	0.00002	0.00001
8	32.0	0.01930	1.0	0.00900	0.00500	0.00002	0.00001
9	31.0	0.02170	1.0	0.00900	0.00500	0.00002	0.00001
10	30.0	0.02410	1.0	0.00900	0.00500	0.00002	0.00001
11	29.0	0.02650	1.0	0.00900	0.00500	0.00002	0.00001
12	28.0	0.02890	1.0	0.00900	0.00500	0.00002	0.00001
13	27.0	0.03130	1.0	0.00900	0.00500	0.00002	0.00001
14	26.0	0.03370	1.0	0.00900	0.00500	0.00002	0.00001
15	25.0	0.03620	1.0	0.00900	0.00500	0.00002	0.00001
16	24.0	0.03860	1.0	0.00900	0.00500	0.00002	0.00001
17	23.0	0.04100	1.0	0.00899	0.00500	0.00002	0.00001
18	22.0	0.04340	1.0	0.00893	0.00498	0.00002	0.00001
19	21.0	0.04610	1.0	0.00852	0.00488	0.00002	0.00001
20	20.0	0.05000	1.0	0.00700	0.00450	0.00002	0.00001
21	19.0	0.05610	1.0	0.00548	0.00412	0.00002	0.00001

Table 2
continued

	P	F	Kr	DU	DTh	DRa	DPa
22	18.0	0.06340	1.0	0.00507	0.00402	0.00002	0.00001
23	17.0	0.07100	1.0	0.00501	0.00400	0.00002	0.00001
24	16.0	0.07860	1.0	0.00500	0.00400	0.00002	0.00001
25	15.0	0.08620	1.0	0.00500	0.00400	0.00002	0.00001
26	14.0	0.09370	1.0	0.00500	0.00400	0.00002	0.00001
27	13.0	0.10133	1.0	0.00500	0.00400	0.00002	0.00001
28	12.0	0.10892	1.0	0.00500	0.00400	0.00002	0.00001
29	11.0	0.11651	1.0	0.00500	0.00400	0.00002	0.00001
30	10.0	0.12410	1.0	0.00500	0.00400	0.00002	0.00001
31	9.0	0.13169	1.0	0.00500	0.00400	0.00002	0.00001
32	8.0	0.13928	1.0	0.00500	0.00400	0.00002	0.00001
33	7.0	0.14687	1.0	0.00500	0.00400	0.00002	0.00001
34	6.0	0.15446	1.0	0.00500	0.00400	0.00002	0.00001
35	5.0	0.16205	1.0	0.00500	0.00400	0.00002	0.00001
36	4.0	0.16964	1.0	0.00500	0.00400	0.00002	0.00001
37	3.0	0.17723	1.0	0.00500	0.00400	0.00002	0.00001
38	2.0	0.18482	1.0	0.00500	0.00400	0.00002	0.00001
39	1.0	0.19241	1.0	0.00500	0.00400	0.00002	0.00001
40	0.0	0.20000	1.0	0.00500	0.00400	0.00002	0.00001

Note. This table illustrates the format required for input files for this model.

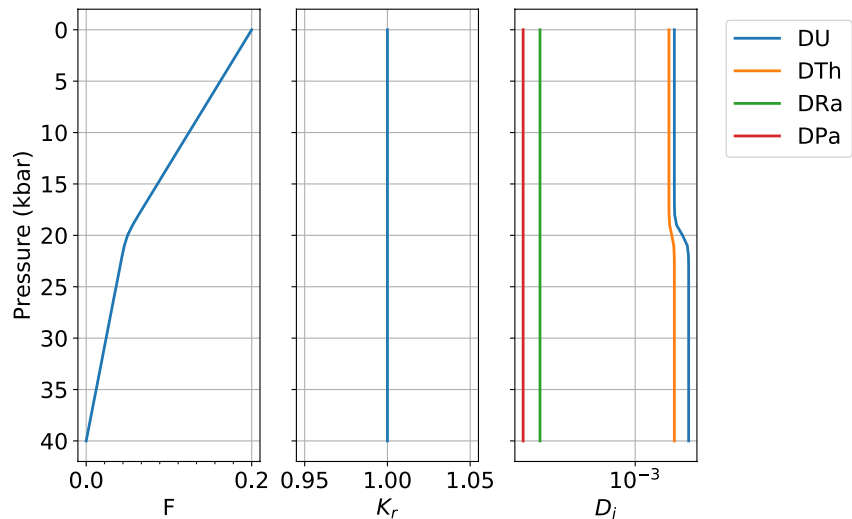


Figure 1. Diagrams showing example input parameters F , K_r , and D_i as a function of pressure, for the sample input file tested here.

3.2.2. Single Column Equilibrium Transport Model

In its default mode, `UserCalc` solves the one-dimensional steady-state equilibrium transport model described in Spiegelman (2000). Below we will initialize the model, solve for a single column and plot the results.

First we set the physical parameters for the upwelling column and initial conditions:


```
[5]: # Maximum melt porosity:
phi0 = 0.008

# Solid upwelling rate in cm/yr. (to be converted to km/yr. in the driver
↳function):
W0 = 3.

# Permeability exponent:
n = 2.

# Solid and liquid densities in kg/m3:
rho_s = 3300.
rho_f = 2800.

# Initial activity values (default is 1.0):
alpha0_238U = 1.
alpha0_235U = 1.
alpha0_230Th = 1.
alpha0_226Ra = 1.
alpha0_231Pa = 1.
alpha0_all = np.array([alpha0_238U, alpha0_230Th, alpha0_226Ra,
↳alpha0_235U, alpha0_231Pa])
```

Next, we initialize the default equilibrium model:

```
[6]: us_eq = UserCalc.UserCalc(df)
```

and run the model for the input code and display the results for the final predicted melt composition in List 1:

```
[7]: df_out_eq = us_eq.solve_all_1D(phi0,n,W0,alpha0_all)
df_out_eq.tail(n=1)
```

```
[7]:      P      z      F      phi (230Th/238U) (226Ra/230Th) (231Pa/235U) Uf_238U
40  0.0  0.0  0.2  0.008  1.164941  1.590091  2.10557  -3.121055

      Uf_230Th Uf_226Ra Us_238U Us_230Th Us_226Ra Uf_235U Uf_231Pa
40 -3.556171 -8.613841 -3.121055 -3.556171 -8.613841 -3.121909 -9.179718

      Us_235U Us_231Pa
40 -3.121909 -9.179718
```

List 1 Model output results for the equilibrium melting scenario tested above.

The cell below produces Figure 2, which shows the model results with depth:

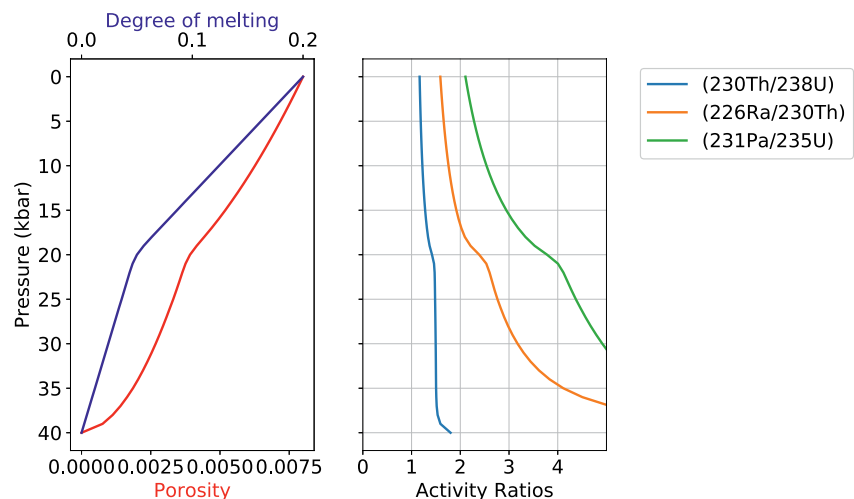


Figure 2. Equilibrium model output results for the degree of melting, residual melt porosity, and activity ratios ($^{230}\text{Th}/^{238}\text{U}$), ($^{226}\text{Ra}/^{230}\text{Th}$), and ($^{231}\text{Pa}/^{235}\text{U}$) as a function of pressure.

```
[8]: fig = UserCalc.plot_1Dcolumn(df_out_eq)
```

3.2.3. Single Column Disequilibrium Transport Model

For comparison, we can repeat the calculation using the disequilibrium transport model, and compare the results to the equilibrium model. We first initialize a new model with $Da = 0$, which will calculate full disequilibrium transport:

```
[9]: us_diseq = UserCalc.UserCalc(df, model=UserCalc.DisequilTransport, Da=0.)
```

The cells below calculate solutions for this pure disequilibrium scenario, as shown in [List 2](#):

```
[10]: df_out = us_diseq.solve_all_1D(phi0,n,W0,alpha0_all)
df_out.tail(n=1)
```

```
[10]:      P      z      F      phi (230Th/238U) (226Ra/230Th) (231Pa/235U) Uf_238U
40  0.0  0.0  0.2  0.008  1.051064      1.001054      1.055847  -3.096744

      Uf_230Th Uf_226Ra  Us_238U  Us_230Th  Us_226Ra  Uf_235U  Uf_231Pa
40 -3.63473 -9.155135 -39.606509 -39.945908 -42.201598 -3.096769 -9.844821

      Us_235U  Us_231Pa
40 -39.602818 -45.46502
```

List 2 Model output results for the disequilibrium melting scenario tested above.

Next we compare the results to our equilibrium calculation above:

```
[11]: fig, axes = UserCalc.plot_1Dcolumn(df_out)
for s in ['(230Th/238U)', '(226Ra/230Th)', '(231Pa/235U)']:
    axes[2].plot(df_out_eq[s], df_out['P'], '--', color='grey')
axes[2].set_title('Da = {}'.format(us_diseq.Da))
plt.show()
```

The dashed gray curves in [Figure 3](#) illustrate the equilibrium transport solution, which is significantly different from the disequilibrium solution. If we increase the value of Da , however, the disequilibrium transport solution should converge toward the equilibrium scenario. To illustrate this, below we calculate the result for $Da = 1$:

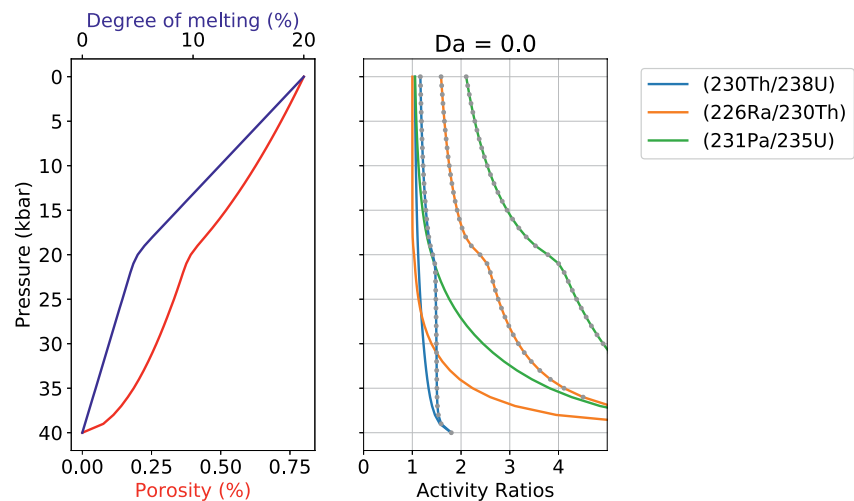


Figure 3. Disequilibrium model output results for the degree of melting, residual melt porosity, and activity ratios ($^{230}\text{Th}/^{238}\text{U}$), ($^{226}\text{Ra}/^{230}\text{Th}$), and ($^{231}\text{Pa}/^{235}\text{U}$) as a function of pressure, for the Damköhler number shown ($Da = 0$). For comparison, the dashed gray curves show solutions for the equilibrium transport model.

```
[12]: # Reset the Da number in the reactive transport model to 1:
us_diseq.Da=1.

# Recalculate the model:
df_out = us_diseq.solve_all_1D(phi0,n,W0,alpha0_all)
df_out_eq.tail(n=1)
```

```
[12]: P z F phi (230Th/238U) (226Ra/230Th) (231Pa/235U) Uf_238U
40 0.0 0.0 0.2 0.008 1.164941 1.590091 2.10557 -3.121055

Uf_230Th Uf_226Ra Us_238U Us_230Th Us_226Ra Uf_235U Uf_231Pa
40 -3.556171 -8.613841 -3.121055 -3.556171 -8.613841 -3.121909 -9.179718

Us_235U Us_231Pa
40 -3.121909 -9.179718
```

List 3 Model output results for the disequilibrium melting scenario tested above, where $Da = 1$.

```
[13]: fig, axes = UserCalc.plot_1Dcolumn(df_out)
for s in ['(230Th/238U)', '(226Ra/230Th)', '(231Pa/235U)']:
    axes[2].plot(df_out_eq[s],df_out['P'],'--',color='grey')
axes[2].set_title('Da = {}'.format(us_diseq.Da))
plt.show()
```

The outcome of the above calculation (Figure 4, List 3) approaches the equilibrium scenario more closely, as predicted. Below is an additional comparison for $Da = 10$:

```
[14]: # Reset the Da number in the reactive transport model to 10:
us_diseq.Da=10.

# Recalculate and plot the model:
df_out = us_diseq.solve_all_1D(phi0,n,W0,alpha0_all)
fig, axes = UserCalc.plot_1Dcolumn(df_out)
for s in ['(230Th/238U)', '(226Ra/230Th)', '(231Pa/235U)']:
    axes[2].plot(df_out_eq[s],df_out['P'],'--',color='grey')
axes[2].set_title('Da = {}'.format(us_diseq.Da))
plt.show()
```

For $Da = 10$ (Figure 5), the activity ratios in the melt are indistinguishable from the equilibrium calculation, suggesting that a Damköhler number of 10 is sufficiently high for a melting system to approach chemical equilibrium,

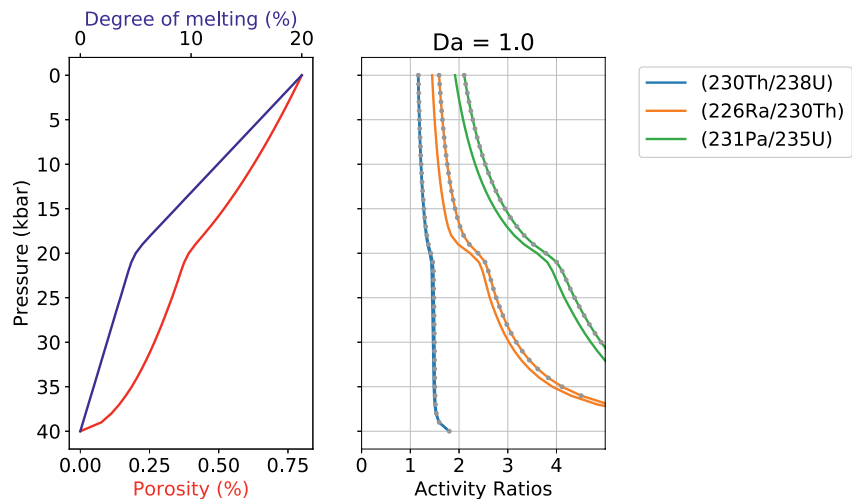


Figure 4. Disequilibrium model output as in Figure 3, but for $Da = 1$.

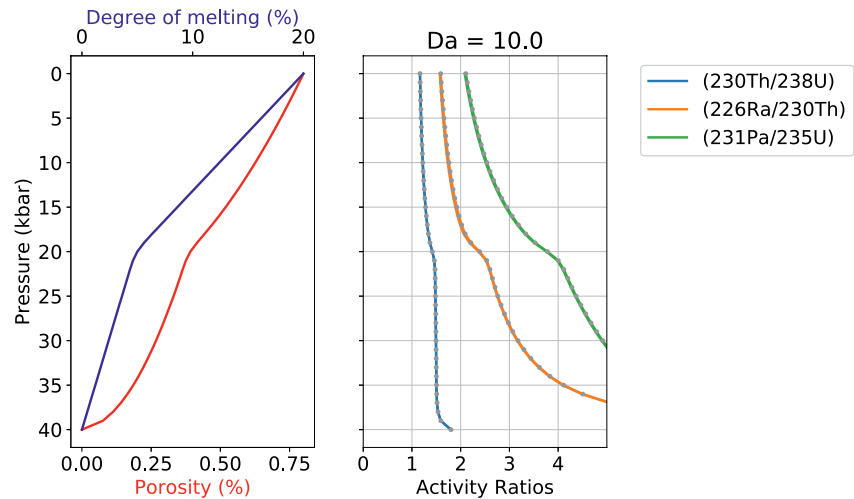


Figure 5. Disequilibrium model output as in Figure 3, but for $Da = 10$.

and illustrating that the equilibrium model of Spiegelman and Elliott (1993) and Spiegelman (2000) is the limiting case for the more general disequilibrium model presented here. For this problem, equilibrium transport always provides an upper bound on activity ratios.

3.2.4. Stable Element Concentrations

For a stable element, that is, $\lambda_i = 0$, Spiegelman and Elliott (1993) showed that the equilibrium melting model reduces identically to simple batch melting (Shaw, 1970), while the disequilibrium model with $Da = 0$ is equivalent to true fractional melting. This presents a useful test of the calculator that verifies the program is correctly calculating stable concentrations. To simulate stable element concentrations for U, Th, Ra, and Pa during equilibrium melting, we can use the same input file example as above and simply test the scenario where λ_i values are equal to zero.

First, we impose a “stable” condition that changes all decay constants $\lambda_i = 0$:

```
[15]: us_eq = UserCalc.UserCalc(df,stable=True)
df_out_eq = us_eq.solve_all_1D(phi0,n,W0,alpha0_all)
df_out_eq.tail(n=1)
```

```
[15]:      P      z      F      phi (230Th/238U) (226Ra/230Th) (231Pa/235U) Uf_238U
40  0.0  0.0  0.2  0.008  1.003937  1.015919  1.019959  -3.120895

      Uf_230Th Uf_226Ra Us_238U Us_230Th Us_226Ra Uf_235U Uf_231Pa
40 -3.704753 -9.21042 -3.120895 -3.704753 -9.21042 -3.120895 -9.903528

      Us_235U Us_231Pa
40 -3.120895 -9.903528
```

List 4 Model output results for equilibrium porous flow melting where $\lambda_i = 0$, simulating stable element behavior for U, Th, Ra, and Pa and thus true (instantaneous) batch melting.

For comparison with the results in List 4, we can use the batch melting equation (Shaw, 1970) to calculate the concentrations of U, Th, Ra, and Pa using the input values in Table 2 for $F(z)$ and D_i , where:

$$\frac{c_i^f}{c_i^0} = \frac{1}{F + D_i(1 - F)} \quad (61)$$

and determine radionuclide activities for the batch melt using the definition of the activity a for a nuclide i :

$$a_i = \lambda_i c_i^f \quad (62)$$

and the initial nuclide activities a_i^0 , such that:

$$a_i = \frac{a_i^0}{F + D_i(1 - F)} \quad (63)$$

As the activity ratios in List 5 illustrate, the outcomes of this simple batch melting equation are identical to those produced by the model for equilibrium transport and $\lambda = 0$.

```
[16]: df_batch=df[['P', 'F', 'DU', 'DTh', 'DRa', 'DPa']]
df_batch['(230Th/238U)'] = (alpha0_all[1]/(df_batch.F-df_batch.F*df_batch.
->DTh+df_batch.DTh))/(alpha0_all[0]/(df_batch.F-df_batch.F*df_batch.
->DU+df_batch.DU))
df_batch['(226Ra/230Th)'] = (alpha0_all[2]/(df_batch.F-df_batch.
->F*df_batch.DRa+df_batch.DRa))/(alpha0_all[1]/(df_batch.F-df_batch.
->F*df_batch.DTh+df_batch.DTh))
df_batch['(231Pa/235U)'] = (alpha0_all[4]/(df_batch.F-df_batch.F*df_batch.
->DPa+df_batch.DPa))/(alpha0_all[3]/(df_batch.F-df_batch.F*df_batch.
->DU+df_batch.DU))

# Extract columns and concatenate dataframes
cols = ['P', 'F', '(230Th/238U)', '(226Ra/230Th)', '(231Pa/235U)']
df_compare = pd.concat([ df_batch[cols].tail(1), df_out_eq[cols].tail(1)])
df_compare['model'] = ['Batch Melting', 'Equilibrium Transport: stable_
->elements']
df_compare.set_index('model')
```

```
[16]:
```

	P	F	(230Th/238U)	(226Ra/230Th)
model				
Batch Melting	0.0	0.2	1.003937	1.015919
Equilibrium Transport: stable elements	0.0	0.2	1.003937	1.015919


```
(231Pa/235U)
```

	P	F	(231Pa/235U)
model			
Batch Melting		1.019959	
Equilibrium Transport: stable elements		1.019959	

List 5 Simple batch melting calculation results using the methods of Shaw (1970), demonstrating identical activity ratio results to those calculated using the equilibrium transport model with $\lambda_i = 0$.

Similarly, we can also determine pure disequilibrium melting using the disequilibrium transport model with $\lambda_i = 0$. A simple fractional melting problem is easiest to test using constant melt productivity and partitioning behavior, so here we test a simplified, one-layer scenario with constant dF/dz and D_i values (Figure 6):

```
[17]: input_file_2 = 'data/simple_sample.csv'
df_test = pd.read_csv(input_file_2, skiprows=1, dtype=float)
UserCalc.plot_inputs(df_test)
df_test.tail(n=1)
```

```
[17]:
```

	P	F	Kr	DU	DTh	DRa	DPa
40	0.0	0.0964	1.0	0.009	0.005	0.00002	0.00001

We note that numerical ODE solvers may not successfully solve for pure fractional melting with $Da = 0$ and stable elements, because the resulting extreme changes in solid concentrations for highly incompatible elements are difficult to resolve using numerical methods. Stable solutions can nonetheless be obtained for very small values of Da that approach $Da = 0$, and such solutions still provide a useful test of the disequilibrium transport model. Here, we use $Da = 10^{-10}$; for such low Da values, the liquid closely approaches the composition of an accumulated fractional melt, and although the liquid and solid outcomes are slightly different from pure fractional melting, the solid is still essentially depleted of all incompatible nuclides.

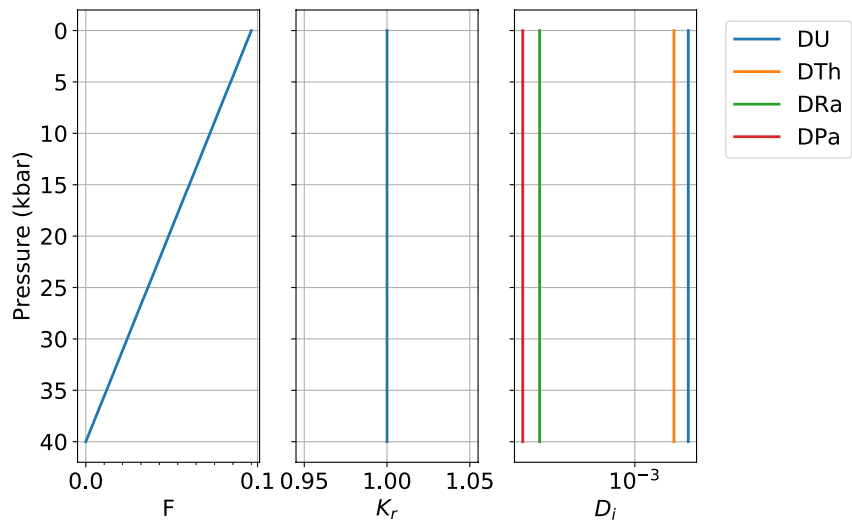


Figure 6. Simple alternative input file with constant melt productivity and constant solid/melt partitioning, used here to test pure fractional melting outputs.

```
[18]: us_diseq_test = UserCalc.UserCalc(df_test, model=UserCalc.  
-DisequilTransport, stable=True, Da=1.e-10)
```

```
[19]: df_diseq_test = us_diseq_test.solve_all_1D(phi0,n,W0,alpha0_all)
```

Similar to our approach for equilibrium and batch melting, we can compare the results of disequilibrium transport for stable elements with pure fractional melting for constant partition coefficients using the definition of aggregated fractional melt concentrations (Figure 7):

$$\frac{c_i^s}{c_i^{s,0}} = (1 - F)^{1/D_i - 1} \quad (64)$$

$$\frac{c_i^f}{c_i^{f,0}} = \frac{D_i}{F} \left(1 - (1 - F)^{1/D_i} \right) \quad (65)$$

or in log units:

$$U_i^s = (1 / D_i - 1) \log(1 - F) \quad (66)$$

$$U_i^f = \log \left(1 - (1 - F)^{1/D_i} \right) + \log \left(\frac{D_i}{F} \right) \quad (67)$$

```
[20]: df_frac=df_test[['P','F','DU','DTh','DRa','DPa']]  
df_frac['(230Th/238U)'] = ((alpha0_all[1]/df_frac.F)*(1.-(1.-df_frac.  
-F)**(1./df_frac.DTh))) / ((alpha0_all[0]/df_frac.F)*(1.-(1.-df_frac.  
-F)**(1./df_frac.DU)))  
df_frac['(226Ra/230Th)'] = ((alpha0_all[2]/df_frac.F)*(1.-(1.-df_frac.  
-F)**(1./df_frac.DRa))) / ((alpha0_all[1]/df_frac.F)*(1.-(1.-df_frac.  
-F)**(1./df_frac.DTh)))  
df_frac['(231Pa/235U)'] = ((alpha0_all[4]/df_frac.F)*(1.-(1.-df_frac.  
-F)**(1./df_frac.DPa))) / ((alpha0_all[3]/df_frac.F)*(1.-(1.-df_frac.  
-F)**(1./df_frac.DU)))
```

```
[21]: fig, axes = UserCalc.plot_1Dcolumn(df_diseq_test)  
for s in ['(230Th/238U)', '(226Ra/230Th)', '(231Pa/235U)']:  
    axes[2].plot(df_frac[s], df_diseq_test['P'], '--', color='black')  
plt.show()
```

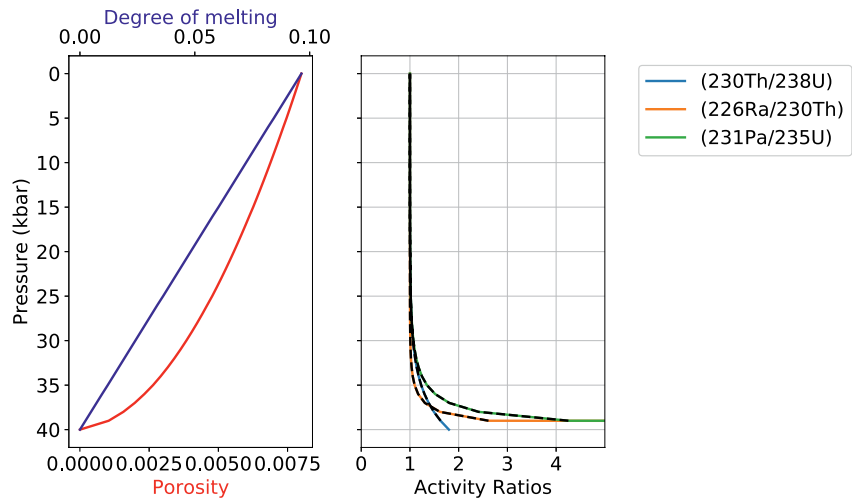


Figure 7. Model output results for the degree of melting, residual melt porosity, and activity ratios ($^{230}\text{Th}/^{238}\text{U}$), ($^{226}\text{Ra}/^{230}\text{Th}$), and ($^{231}\text{Pa}/^{235}\text{U}$) as a function of pressure. The solid curves plot the results of pure fractional melting for stable elements, while the dashed black curves illustrate the outcomes of the disequilibrium transport model with $Da = 10^{-10}$ and $\lambda_i = 0$. The outcomes of the two methods are indistinguishable.

3.2.5. Considering Lithospheric Transport Scenarios

In mantle decompression melting scenarios, melting is expected to cease in the shallow, colder part of the regime where a lithospheric layer is present. The effects of cessation of melting prior to reaching the surface can be envisioned as affecting magma compositions in a number of ways, some of which could be calculated using the models presented here by setting $dF = 0$.

There are, however, several limitations when using our transport models to simulate lithospheric melt transport in this way, as the model equations are written to track steady-state decompression and melting. The first limitation is thus the underlying assumption that the solid is migrating and experiences progressive melt depletion in the model, while the solid lithosphere should in fact behave as a rigid matrix that does not experience upwelling. For the disequilibrium transport model with $Da = 0$, no chemical reequilibration occurs while $dF = 0$, so the lack of solid migration after the cessation of melting does not pose a problem; instead, in the pure disequilibrium transport case, imposing $dF = 0$ simply allows for radioactive decay and ingrowth during transport through the lithospheric layer.

The equilibrium transport model, on the other hand, permits full equilibration even if $dF = 0$, but the liquid composition does not directly depend on the solid concentration, $c_i^s(z)$, so ongoing chemical reequilibration between the liquid and a modified lithospheric solid could be simulated by modifying the bulk solid/liquid partition coefficients D_i . However, the underlying model assumes that the liquid with mass proportion F_{max} reequilibrates with the solid matrix in a steady-state transport regime, at the maximum reference porosity, which may not accurately simulate the transport regime through the fixed lithosphere with no melting. Because it does not directly consider mineral abundances or compositions, the model also does not account for complexities such as low temperature melt-rock reaction or mineral growth.

The case of the scaled disequilibrium transport model with $Da > 0$ is the most complex, since the model directly calculates reequilibration of the liquid with a progressively melting solid layer, and thus may not accurately simulate transport through the fixed solid lithosphere. We advise that if the model is used in this way, the results must be interpreted with additional caution.

Finally, calculating a given transport model through the upwelling asthenosphere and into a fixed overlying lithospheric layer neglects an additional, significant limitation: namely that melt-rock interactions, and thus the magma transport style, may be different in the lithosphere than in the melting asthenosphere. As noted above, this could also include low-temperature reactions and the growth of new mineral phases. While it is not possible to change transport models during a single 1D run in the current implementation, one alternative approach is to

change the relative permeability, K_r , in the lithosphere, in addition to modifying the bulk partition coefficients to reflect lithospheric values. It may also be possible to run a separate, second-stage lithospheric calculation with modified input parameters and revised liquid porosity constraints, but this option is not currently implemented and would require an expansion of the current model.

Despite these caveats, there are some limited scenarios where users may wish to simulate equilibrium or disequilibrium magma transport through a capping layer with constant $dF = 0$, constant $\phi = \phi_0$, and revised D_i values for a modified layer mineralogy. The cells below provide options for modifying the existing input data table to impose such a layer. The first cell identifies a final melting pressure P_{Lithos} , which is defined by the user in kbar. This value can be set to 0.0 if no lithospheric cap is desired; in the example below, it has been set at 5.0 kbar. There are two overall options for how this final melting pressure could be used to modify the input data. The first option (implemented in Supporting Information S1 but not tested here) simply deletes all lines in the input dataframe for depths shallower than P_{Lithos} . This is a straightforward option for a one-dimensional column scenario, where melting simply stops at the base of the lithosphere and the composition of the melt product is observed in that position. This is an effective way to limit further chemical interactions after melting has ceased; it fails to account for additional radioactive decay during lithospheric melt transport, but subsequent isotopic decay over a fixed transport time interval could then be calculated using the radioactive decay equations for U-series nuclides.

A second option, shown here to demonstrate outcomes, changes the degree of melting increments (dF) to a value of 0 for all depths shallower than P_{Lithos} , but allows model calculations to continue at shallower depths. This is preferable if the user aims to track additional radioactive decay and/or chemical exchange after melting has ceased and during subsequent transport through the lithospheric layer, and shall be explored further below.

```
[22]: Plithos = 5.0

Pfinal = df.iloc[(df['P']-Plithos).abs().idxmin()]
F_max = Pfinal[1].tolist()
df.loc[(df['P'] < Plithos),['F']] = F_max
```

For equilibrium transport scenarios, the cell below offers one possible option for modifying lithospheric solid/melt bulk partition coefficients. We note that if the disequilibrium transport model is used with $Da = 0$ (i.e., pure chemical disequilibrium), this cell is not necessary.

The option demonstrated below imposes new, constant melt-rock partition coefficients during lithospheric transport. These values are assumed to be fixed. An alternative choice, included in Supporting Information S1, instead fixes the shallower lithospheric solid/melt bulk partition coefficients such that they are equal to D_i values at the depth where melting ceased (i.e., P_{Lithos}).

```
[23]: # Define new bulk solid/liquid partition coefficients for the
      # lithospheric layer:
      D_U_lith = 0.002
      D_Th_lith = 0.006
      D_Ra_lith = 0.00002
      D_Pa_lith = 0.00001

      # Implement the changed values defined above:
      df.loc[(df['P'] < Plithos),['DU']] = D_U_lith
      df.loc[(df['P'] < Plithos),['DTh']] = D_Th_lith
      df.loc[(df['P'] < Plithos),['DRa']] = D_Ra_lith
      df.loc[(df['P'] < Plithos),['DPa']] = D_Pa_lith
```

Following any changes implemented above, the cells below will process and display the refined input data (Figure 8 and Table 3).

```
[24]: UserCalc.plot_inputs(df)
```

```
[25]: df
```

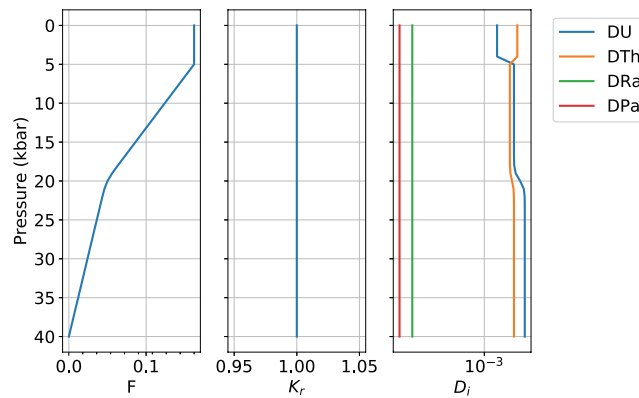



Figure 8. Diagrams showing input parameters F , K_r , and D_i as a function of pressure, for example, the input file and modified lithospheric conditions.

Table 3

Input Data Table for an Example Scenario With Modified Lithospheric Transport Conditions, Showing Pressures in kbar (P), Degree of Melting (F), Permeability Coefficient (K_r), and Bulk Solid/Melt Partition Coefficients (D_i) for the Elements of Interest, U , Th , Ra , and Pa

	P	F	Kr	DU	DTh	DRa	DPa
0	40.0	0.00000	1.0	0.00900	0.00500	0.00002	0.00001
1	39.0	0.00241	1.0	0.00900	0.00500	0.00002	0.00001
2	38.0	0.00482	1.0	0.00900	0.00500	0.00002	0.00001
3	37.0	0.00723	1.0	0.00900	0.00500	0.00002	0.00001
4	36.0	0.00964	1.0	0.00900	0.00500	0.00002	0.00001
5	35.0	0.01210	1.0	0.00900	0.00500	0.00002	0.00001
6	34.0	0.01450	1.0	0.00900	0.00500	0.00002	0.00001
7	33.0	0.01690	1.0	0.00900	0.00500	0.00002	0.00001
8	32.0	0.01930	1.0	0.00900	0.00500	0.00002	0.00001
9	31.0	0.02170	1.0	0.00900	0.00500	0.00002	0.00001
10	30.0	0.02410	1.0	0.00900	0.00500	0.00002	0.00001
11	29.0	0.02650	1.0	0.00900	0.00500	0.00002	0.00001
12	28.0	0.02890	1.0	0.00900	0.00500	0.00002	0.00001
13	27.0	0.03130	1.0	0.00900	0.00500	0.00002	0.00001
14	26.0	0.03370	1.0	0.00900	0.00500	0.00002	0.00001
15	25.0	0.03620	1.0	0.00900	0.00500	0.00002	0.00001
16	24.0	0.03860	1.0	0.00900	0.00500	0.00002	0.00001
17	23.0	0.04100	1.0	0.00899	0.00500	0.00002	0.00001
18	22.0	0.04340	1.0	0.00893	0.00498	0.00002	0.00001
19	21.0	0.04610	1.0	0.00852	0.00488	0.00002	0.00001
20	20.0	0.05000	1.0	0.00700	0.00450	0.00002	0.00001
21	19.0	0.05610	1.0	0.00548	0.00412	0.00002	0.00001
22	18.0	0.06340	1.0	0.00507	0.00402	0.00002	0.00001
23	17.0	0.07100	1.0	0.00501	0.00400	0.00002	0.00001
24	16.0	0.07860	1.0	0.00500	0.00400	0.00002	0.00001
25	15.0	0.08620	1.0	0.00500	0.00400	0.00002	0.00001
26	14.0	0.09370	1.0	0.00500	0.00400	0.00002	0.00001
27	13.0	0.10133	1.0	0.00500	0.00400	0.00002	0.00001

Table 3
continued

	P	F	Kr	DU	DTh	DRa	DPa
28	12.0	0.10892	1.0	0.00500	0.00400	0.00002	0.00001
29	11.0	0.11651	1.0	0.00500	0.00400	0.00002	0.00001
30	10.0	0.12410	1.0	0.00500	0.00400	0.00002	0.00001
31	9.0	0.13169	1.0	0.00500	0.00400	0.00002	0.00001
32	8.0	0.13928	1.0	0.00500	0.00400	0.00002	0.00001
33	7.0	0.14687	1.0	0.00500	0.00400	0.00002	0.00001
34	6.0	0.15446	1.0	0.00500	0.00400	0.00002	0.00001
35	5.0	0.16205	1.0	0.00500	0.00400	0.00002	0.00001
36	4.0	0.16205	1.0	0.00500	0.00400	0.00002	0.00001
37	3.0	0.16205	1.0	0.00500	0.00400	0.00002	0.00001
38	2.0	0.16205	1.0	0.00500	0.00400	0.00002	0.00001
39	1.0	0.16205	1.0	0.00500	0.00400	0.00002	0.00001
40	0.0	0.16205	1.0	0.00500	0.00400	0.00002	0.00001

The cells below will rerun the end member models for the modified lithospheric input file. First, equilibrium transport:

```
[26]: us_eq = UserCalc.UserCalc(df,stable=False)
df_out_eq = us_eq.solve_all_1D(phi0,n,W0,alpha0_all)
```

And second, for disequilibrium transport with $Da = 0$:

```
[27]: us_diseq = UserCalc.UserCalc(df,model=UserCalc.
    .DisequilTransport, Da=0, stable=False)
df_out_diseq = us_diseq.solve_all_1D(phi0,n,W0,alpha0_all)
```

List 6 below displays the activity ratios determined for the final melt compositions at the end of the two simulations (i.e., the tops of the one-dimensional melting columns).

```
[28]: df_compare = pd.concat([df_out_eq.tail(n=1), df_out_diseq.tail(n=1)])
df_compare['model'] = ['Equilibrium Transport', 'Disequilibrium Transport']
df_compare.set_index('model')
```

```
[28]:
```

	P	z	F	phi	(230Th/238U)		
model							
Equilibrium Transport	0.0	0.0	0.16205	0.008	1.015792		
Disequilibrium Transport	0.0	0.0	0.16205	0.008	1.039704		
						(226Ra/230Th)	(231Pa/235U) Uf_238U Uf_230Th
model							
Equilibrium Transport			1.894057		1.792975	-2.901132	-3.473250
Disequilibrium Transport			1.000828		1.034719	-2.891833	-3.440684
						Uf_226Ra	Us_238U Us_230Th Us_226Ra Uf_235U
model							
Equilibrium Transport	-8.355990	-2.901132			-3.473250	-8.355990	-2.902001
Disequilibrium Transport	-8.96132	-30.351986			-30.353121	-30.353146	-2.88492
						Uf_231Pa	Us_235U Us_231Pa
model							
Equilibrium Transport	-9.120520				-2.902001	-9.120520	
Disequilibrium Transport	-9.653185				-30.272812	-30.272749	

List 6 Model output results for the disequilibrium ($Da = 0$) melting scenarios tested here, with modified lithospheric input conditions.

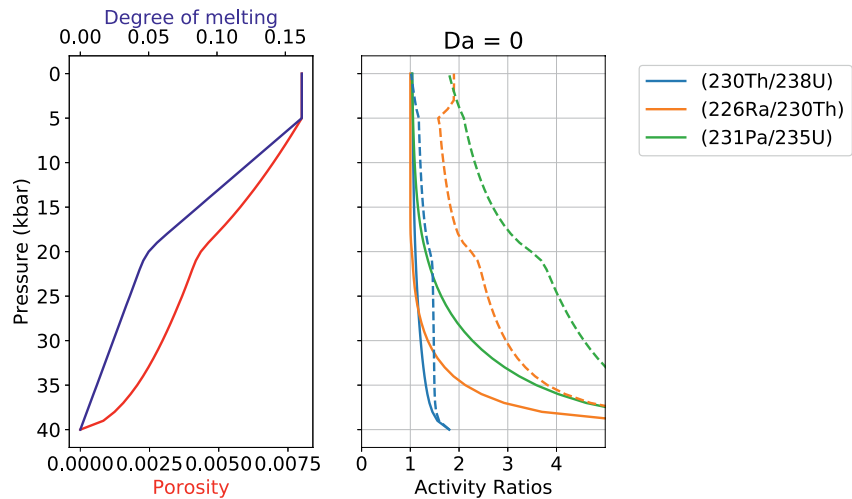


Figure 9. Comparison of equilibrium (dashed) and disequilibrium ($Da = 0$; solid) transport model output results for the degree of melting, residual melt porosity, and activity ratios ($^{230}\text{Th}/^{238}\text{U}$), ($^{226}\text{Ra}/^{230}\text{Th}$), and ($^{231}\text{Pa}/^{235}\text{U}$) as a function of pressure, for the modified lithospheric transport scenario explored above. Symbols and lines as in Figure 3.

The following cell generates Figure 9, which illustrates outcomes with depth for the equilibrium and disequilibrium transport models. The model outcomes for the two transport scenarios are notably different, particularly for the shorter-lived isotopic pairs.

```
[29]: fig, axes = UserCalc.plot_1Dcolumn(df_out_diseq)
      axes[2].set_prop_cycle(None)
      for s in ['(230Th/238U)', '(226Ra/230Th)', '(231Pa/235U)']:
          axes[2].plot(df_out_eq[s], df_out['P'], '--')
      axes[2].set_title('Da = {}'.format(us_diseq.Da))
      plt.show()
```

3.3. Batch Operations

For many applications, it is preferable to calculate an ensemble of model scenarios over a range of input parameters directly related to questions about the physical constraints on melt generation, such as the maximum residual or reference melt porosity (ϕ_0) and the solid mantle upwelling rate (W_0). The cells below determine a series of one-dimensional column results for the equilibrium transport model and the parameters defined above (that is, the input conditions shown in Table 3 with $n = 2$, $\rho_s = 3300 \text{ kg/m}^3$, and $\rho_f = 2800 \text{ kg/m}^3$), but over a range of values for ϕ_0 and W_0 ; these results are then shown in a series of figures. The user can select whether to define the specific ϕ_0 and W_0 values as evenly spaced log grid intervals (option 1) or with manually specified values (option 2). As above, all upwelling rates are entered in units of cm/yr. We note that because some of these models tend to be stiff and the Radau solver is relatively computationally expensive, the batch operations below may require a few minutes of computation time for certain scenarios. Here we show the results for the default equilibrium model over a range of selected ϕ_0 and W_0 values:

```
[30]: # Option 1 (evenly spaced log grid intervals):
# phi0 = np.logspace(-3,-2,11)
# W0 = np.logspace(-1,1,11)

# Option 2 (manual selection of values):
phi0 = np.array([0.001, 0.002, 0.005, 0.01])
W0 = np.array([0.5, 1., 2., 5., 10., 20., 50.])

import time
tic = time.perf_counter()
toc = time.perf_counter()

# Calculate the U-238 decay chain grid values:
act = us_eq.solve_grid(phi0, n, W0, us_eq.D_238, us_eq.lambdas_238, us_eq.
    -alphas_238)
Th = act[0]
Ra = act[1]
df = pd.DataFrame(Th)
df = pd.DataFrame(Ra)
```

```
W = 0.5 . . . .
W = 1.0 . . . .
W = 2.0 . . . .
W = 5.0 . . . .
W = 10.0 . . . .
W = 20.0 . . . .
W = 50.0 . . . .
```

```
[31]: # Calculate the U-235 decay chain grid values:
act_235 = us_eq.solve_grid(phi0, n, W0, us_eq.D_235, us_eq.lambdas_235,
    -us_eq.alphas_235)
Pa = act_235[0]
df = pd.DataFrame(Pa)
```

```
W = 0.5 . . . .
W = 1.0 . . . .
W = 2.0 . . . .
W = 5.0 . . . .
W = 10.0 . . . .
W = 20.0 . . . .
W = 50.0 . . . .
```

The figures below illustrate the batch model results in a variety of ways. First, each isotopic activity ratio is contoured in ϕ_0 versus W_0 space (Figure 10), using figures similar to the contour plots of Spiegelman (2000). The model outcomes for W_0 and ϕ_0 values are also contoured as mesh “grids” in activity ratio-activity ratio plots (Figure 11). These diagrams show the outcomes for model runs with a given W_0 and ϕ_0 value at each grid intersection point, and each curve shows outcomes for a constant W_0 value with variable ϕ_0 or vice versa, as indicated in the figure legend. Because this particular example shows results for the equilibrium transport model, and the input values for the shallow, spinel peridotite layer of the sample input file define $D_U < D_{Th}$, we note that some of the results exhibit $(^{230}\text{Th}/^{238}\text{U}) < 1.0$ in Figure 11.

```
[32]: UserCalc.plot_contours(phi0,W0,act, figsize=(12,12))
```

```
[33]: UserCalc.plot_contours(phi0,W0,act_235)
```

```
[34]: UserCalc.plot_mesh_Ra(Th,Ra,W0,phi0)
```

```
[35]: UserCalc.plot_mesh_Pa(Th,Pa,W0,phi0)
```

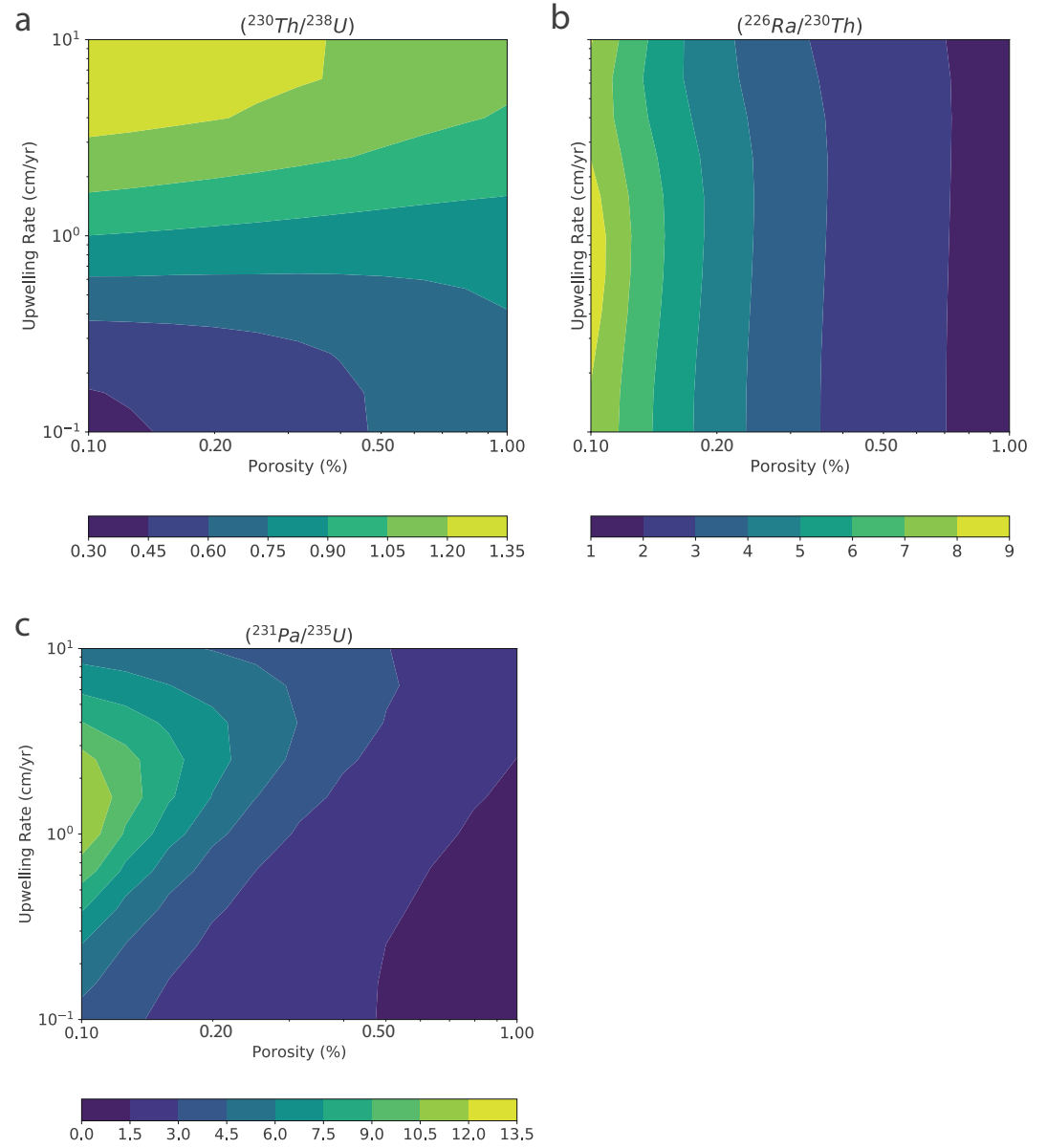


Figure 10. Diagrams of upwelling rate (W_0) versus maximum residual melt porosity (ϕ) showing contoured activity ratios for (a) $(^{230}\text{Th}/^{238}\text{U})$, (b) $(^{226}\text{Ra}/^{230}\text{Th})$, and (c) $(^{231}\text{Pa}/^{235}\text{U})$.

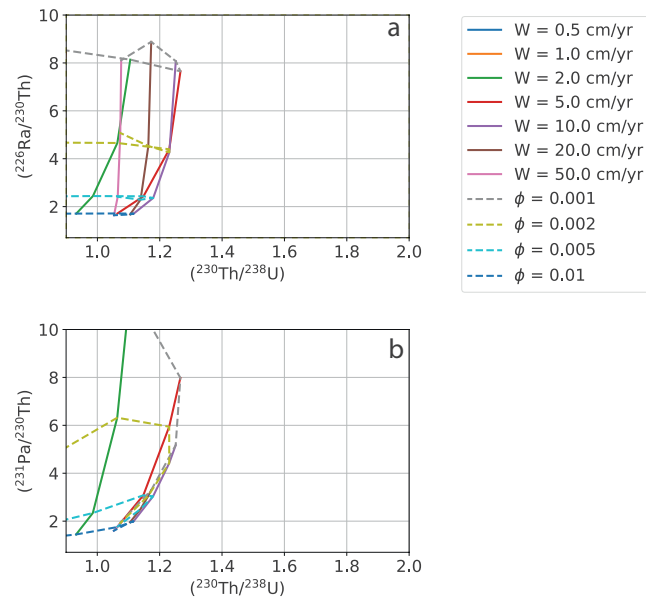


Figure 11. Diagrams showing (a) $(^{226}\text{Ra}/^{230}\text{Th})$ versus $(^{230}\text{Th}/^{238}\text{U})$ and (b) $(^{231}\text{Pa}/^{230}\text{Th})$ versus $(^{230}\text{Th}/^{238}\text{U})$ for the gridded upwelling rate (W_0) and maximum residual porosity (ϕ) values defined above.

4. Summary

We present pyUserCalc, an expanded, publicly available, open-source version of the UserCalc code for determining U-series disequilibria generated in basalts by one-dimensional, decompression partial melting. The model has been developed from conservation of mass equations with two-phase (solid and liquid) porous flow and permeability governed by Darcy's Law. The model reproduces the functionality of the original UserCalc equilibrium porous flow calculator (Spiegelman, 2000) in pure Python code, and implements a new disequilibrium transport model. The disequilibrium transport code includes reactivity rate-limited chemical equilibration calculations controlled by a Damköhler number, Da . For stable elements with decay constants equal to zero, the equilibrium model reduces to batch melting and the disequilibrium transport model with $Da = 0$ to pure fractional melting. The method presented here can be extended to other applications in geochemical porous flow calculations in future work.

Acknowledgments

The authors thank two anonymous reviewers for thoughtful feedback that strengthened this manuscript. The authors thank K. W. W. Sims and P. Kelemen for initiating early discussions about creating a new porous flow disequilibrium transport calculator back in 2008. The authors also thank M. Ghiorso for inviting L. Elkins to join the ENKI working group and thereby catalyzing this fresh effort, and we further thank the working group for their helpful suggestions and feedback. L. Elkins received ENKI working group travel assistance that contributed to this research effort, and was supported by NSF award OCE-1658011. M. Spiegelman was supported by the ENKI NSF SI² award NSF-ACI1550337. This work is dedicated to the memory of our colleague, mentor, and friend Peter Fox, who encouraged our work on this project, expertly handled this manuscript, and spearheaded exciting innovations like publishing executable code in "Earth and Space Science."

Data Availability Statement

The data set for this research consists of a code package, which is available in several ways: (a) in the Supporting Information S1, (b) through a binder container (at https://mybinder.org/v2/gl/ENKI-portal%2FpyUsercalc/master?filepath=pyUserCalc_manuscript.ipynb), and (c) in the ENKI GitLab data repository (<https://gitlab.com/ENKI-portal/pyUsercalc>), which can also be accessed at the ENKI cloud server (<https://server.enki-portal.org/hub/login>) with a free GitLab account (register at <https://gitlab.com/ENKI-portal>). The primary source for pyUserCalc is also hosted in the ENKI GitLab repository, and any future issues and merge requests will be handled there.

References

- Aharonov, E., Whitehead, J. A., Kelemen, P., & Spiegelman, M. (1995). Channeling instability of upwelling melt in the mantle. *Journal of Geophysical Research: Solid Earth*, 100(B10), 20433–20450. <https://doi.org/10.1029/95jb01307>
- Bourdon, B., Turner, S. P., & Ribe, N. M. (2005). Partial melting and upwelling rates beneath the Azores from a U-series isotope perspective. *Earth and Planetary Science Letters*, 239, 42–56. <https://doi.org/10.1016/j.epsl.2005.08.008>
- Elkins, L. J., Bourdon, B., & Lambart, S. (2019). Testing pyroxenite versus peridotite sources for marine basalts using U-series isotopes. *Lithos*, 332–333, 226–244. <https://doi.org/10.1016/j.lithos.2019.02.011>
- Feineman, M. D., & DePaolo, D. J. (2003). Steady-state $^{226}\text{Ra}/^{230}\text{Th}$ disequilibrium in mantle minerals: Implications for melt transport rates in island arcs. *Earth and Planetary Science Letters*, 215(3–4), 339–355. [https://doi.org/10.1016/s0012-821x\(03\)00454-0](https://doi.org/10.1016/s0012-821x(03)00454-0)

- Grose, C. J., & Afonso, J. C. (2019). Chemical disequilibria, lithospheric thickness, and the source of ocean island basalts. *Journal of Petrology*, 60(4), 755–790. <https://doi.org/10.1093/ptrology/egz012>
- Iwamori, H. (1993). Dynamic disequilibrium melting model with porous flow and diffusion-controlled chemical equilibration. *Earth and Planetary Science Letters*, 114(2–3), 301–313. [https://doi.org/10.1016/0012-821x\(93\)90032-5](https://doi.org/10.1016/0012-821x(93)90032-5)
- Iwamori, H. (1994). ^{238}U - ^{230}Th - ^{226}Ra and ^{235}U - ^{231}Pa disequilibria produced by mantle melting with porous and channel flows. *Earth and Planetary Science Letters*, 125, 1–16. [https://doi.org/10.1016/0012-821x\(94\)90203-8](https://doi.org/10.1016/0012-821x(94)90203-8)
- Jull, M., Kelemen, P., & Sims, K. (2002). Consequences of diffuse and channelled porous melt migration on uranium series disequilibria. *Geochimica et Cosmochimica Acta*, 66, 4133–4148. [https://doi.org/10.1016/s0016-7037\(02\)00984-5](https://doi.org/10.1016/s0016-7037(02)00984-5)
- Kogiso, T., Hirschmann, M. M., & Reiners, P. W. (2004). Length scales of mantle heterogeneities and their relationship to ocean island basalt geochemistry. *Geochimica et Cosmochimica Acta*, 68(2), 345–360. [https://doi.org/10.1016/s0016-7037\(03\)00419-8](https://doi.org/10.1016/s0016-7037(03)00419-8)
- Liang, Y., & Liu, B. (2016). Simple models for disequilibrium fractional melting and batch melting with application to REE fractionation in abyssal peridotites. *Geochimica et Cosmochimica Acta*, 173, 181–197. <https://doi.org/10.1016/j.gca.2015.10.020>
- Lundstrom, C., Gill, J., & Williams, Q. (2000). A geochemically consistent hypothesis for MORB generation. *Chemical Geology*, 162(2), 105–126. [https://doi.org/10.1016/s0009-2541\(99\)00122-9](https://doi.org/10.1016/s0009-2541(99)00122-9)
- McKenzie, D. (1985). Th- ^{230}U - ^{238}U disequilibrium and the melting processes beneath ridge axes. *Earth and Planetary Science Letters*, 72(2–3), 149–157. [https://doi.org/10.1016/0012-821x\(85\)90001-9](https://doi.org/10.1016/0012-821x(85)90001-9)
- Miller, K. J., Zhu, W. L., Montési, L. G., & Gaetani, G. A. (2014). Experimental quantification of permeability of partially molten mantle rock. *Earth and Planetary Science Letters*, 388, 273–282.
- Oliveira, B., Afonso, J. C., & Tilhac, R. (2020). A disequilibrium reactive transport model for mantle magmatism. *Journal of Petrology*. <https://doi.org/10.1093/ptrology/egaa067>
- Peate, D. W., & Hawkesworth, C. J. (2005). U series disequilibria: Insights into mantle melting and the timescales of magma differentiation. *Reviews of Geophysics*, 43(1). <https://doi.org/10.1029/2004rg000154>
- Qin, Z., Lu, F., & Anderson, A. T. (1992). Diffusive reequilibration of melt and fluid inclusions. *American Mineralogist*, 77(5–6), 565–576.
- Shaw, D. M. (1970). Trace element fractionation during anatexis. *Geochimica et Cosmochimica Acta*, 34(2), 237–243. [https://doi.org/10.1016/0016-7037\(70\)90009-8](https://doi.org/10.1016/0016-7037(70)90009-8)
- Sims, K. W. W., DePaolo, D. J., Murrell, M. T., Baldrige, W. S., Goldstein, S., Clague, D., & Jull, M. (1999). Porosity of the melting zone and variations in the solid mantle upwelling rate beneath Hawaii: Inferences from U- ^{238}Th - ^{230}Ra - ^{226}U and U- ^{235}Pa - ^{231}U disequilibria. *Geochimica et Cosmochimica Acta*, 63(23–24), pp. 4119–4138. [https://doi.org/10.1016/s0016-7037\(99\)00313-0](https://doi.org/10.1016/s0016-7037(99)00313-0)
- Sims, K. W. W., Goldstein, S. J., Blichert-toft, J., Perfit, M. R., Kelemen, P., Fornari, D. J., et al. (2002). Chemical and isotopic constraints on the generation and transport of magma beneath the East Pacific Rise. *Geochimica et Cosmochimica Acta*, 66(19), 3481–3504. [https://doi.org/10.1016/s0016-7037\(02\)00909-2](https://doi.org/10.1016/s0016-7037(02)00909-2)
- Spiegelman, M. (2000). UserCalc: A web-based uranium series calculator for magma migration problems. *Geochemistry, Geophysics, Geosystems*, 1(8), 1016. <https://doi.org/10.1029/1999gc000030>
- Spiegelman, M., & Elliott, T. (1993). Consequences of melt transport for uranium series disequilibrium in young lavas. *Earth and Planetary Science Letters*, 118(1–4), 1–20. [https://doi.org/10.1016/0012-821x\(93\)90155-3](https://doi.org/10.1016/0012-821x(93)90155-3)
- Spiegelman, M., & Kenyon, P. (1992). The requirements for chemical disequilibrium during magma migration. *Earth and Planetary Science Letters*, 109(3–4), 611–620. [https://doi.org/10.1016/0012-821x\(92\)90119-g](https://doi.org/10.1016/0012-821x(92)90119-g)
- Stracke, A., & Bourdon, B. (2009). The importance of melt extraction for tracing mantle heterogeneities. *Geochimica et Cosmochimica Acta*, 73, 218–238. <https://doi.org/10.1016/j.gca.2008.10.015>
- Stracke, A., Zindler, A., Salters, V. J. M., McKenzie, D., & Gronvold, K. (2003). The dynamics of melting beneath Theistareykir, northern Iceland. *Geochemistry, Geophysics, Geosystems*, 4, 8513. <https://doi.org/10.1029/2002gc000347>
- Van Orman, J. A., Grove, T. L., & Shimizu, N. (2002). Diffusive fractionation of trace elements during production and transport of melting in the Earth's upper mantle. *Earth and Planetary Science Letters*, 198, 93–112. [https://doi.org/10.1016/s0012-821x\(02\)00492-2](https://doi.org/10.1016/s0012-821x(02)00492-2)
- Van Orman, J. A., Saal, A. E., Bourdon, B., & Hauri, E. H. (2006). Diffusive fractionation of U-series radionuclides during mantle melting and shallow-level melt-cumulate interaction. *Geochimica et Cosmochimica Acta*, 70(18), 4797–4812. <https://doi.org/10.1016/j.gca.2006.07.005>
- Yang, Z., Sista, S., Elmer, J. W., & DebRoy, T. (2000). Three dimensional Monte Carlo simulation of grain growth during GTA welding of titanium. *Acta Materialia*, 48(20), 4813–4825. [https://doi.org/10.1016/s1359-6454\(00\)00279-2](https://doi.org/10.1016/s1359-6454(00)00279-2)
- Zou, H., & Zindler, A. (2000). Theoretical studies of ^{238}U - ^{230}Th - ^{226}Ra and ^{235}U - ^{231}Pa disequilibria in young lavas produced by mantle melting. *Geochimica et Cosmochimica Acta*, 64(10), 1809–1817. [https://doi.org/10.1016/s0016-7037\(00\)00350-1](https://doi.org/10.1016/s0016-7037(00)00350-1)